

Deep inelastic scattering off scalar mesons in the $1/N$ expansion from the D3D7-brane system

David Jorjin¹, Nicolas Kovensky², and Martin Schvellinger³

Instituto de Física La Plata-UNLP-CONICET

and

*Departamento de Física, Facultad de Ciencias Exactas, Universidad Nacional de La Plata.
Calle 49 y 115, C.C. 67, (1900) La Plata, Buenos Aires, Argentina.*

Abstract

Deep inelastic scattering (DIS) of charged leptons off scalar mesons in the $1/N$ expansion is studied by using the gauge/gravity duality. We focus on the D3D7-brane system and investigate the corresponding structure functions by considering both the high energy limit and the $1/N$ expansion. These limits do not commute. From the D7-brane DBI action we derive a Lagrangian at sub-leading order in the D7-brane fluctuations and obtain a number of interactions some of which become relevant for two-hadron final-state DIS. By considering first the high energy limit followed by the large N one, our results fit lattice QCD data within 1.27% for the first three moments of F_2 for the lightest pseudoscalar meson.

¹jorjin@fisica.unlp.edu.ar

²nico.koven@fisica.unlp.edu.ar

³martin@fisica.unlp.edu.ar

Contents

1	Introduction	2
2	The interaction Lagrangian	6
2.1	Derivation of the interaction Lagrangian from the D7-brane DBI-action	6
2.2	Solutions of the equations of motion	10
3	The leading diagram in the $1/N$ expansion	13
3.1	DIS and comments on the FCS tree-level calculation	13
3.2	The leading diagram for the one-loop FCS calculation	14
3.3	The UV interaction vertex	17
3.4	The IR interaction vertex	18
3.5	Calculation of the structure functions	20
4	Discussion and conclusions	24
A	Spherical harmonics on S^3	31
A.1	Basic properties of spherical harmonics	31
A.2	Integrals of spherical harmonics	32
B	Contribution of the type III mode	33
C	Integrals of products of Bessel functions	34

1 Introduction

Dp-brane models for holographic mesons lead to very interesting results describing masses of the low-lying mesons, meson interactions, as well as other important properties obtained in the large N limit of their corresponding dual confining gauge field theories at strong coupling [1, 2, 3]. These models include the description of quarks in the fundamental representation of the gauge group by using flavor Dp-branes in the probe approximation. However, we should note that there is no holographic dual model which exactly represents all properties of real QCD, even at large N . In particular, for the referred Dp-brane models we can comment on some of their main differences with respect to large N QCD as follows. The Sakai-Sugimoto model [3] is built out of N D4-branes in type IIA superstring theory, by adding N_f D8-branes and N_f $\overline{\text{D8}}$ -branes in the probe approximation. The most important property of this model is that it gives a geometric realization of the chiral symmetry breaking. Recall that antiperiodic boundary conditions for the fermions are imposed on an S^1 where one of the spatial directions of the D4-brane is wrapped, thus supersymmetry is completely broken. At low energy this model describes several properties as QCD does for mesons in the large N limit. At high energy, on the other hand, the size of the circumference grows, which implies that the Kaluza-Klein modes become relevant. This is a signal that the dual gauge theory becomes a five-dimensional one. Moreover, the existence of an S^4 in the ten-dimensional superstring theory background leads to a global $SO(5)$ symmetry which is absent in QCD. Neither the model based on N D4-branes and flavor D6-branes in type IIA superstring theory represents real QCD at its full extent [2]. In addition, the D3D7-brane model in type IIB superstring theory that we investigate in the present work is the holographic dual description of the $SU(N)$ $\mathcal{N} = 2$ supersymmetric Yang-Mills theory in four dimensions, in the multicolor limit and at strong coupling, with quarks in the fundamental representation of the gauge group [1]. Another property which distinguishes between the D3D7-brane model and QCD is that the D3D7-brane system does not lead to any geometric realization of chiral symmetric breaking.

Thus, none of the mentioned Dp-brane models are exact holographic dual models of the large N limit of QCD. However, as we have shown in [4, 5, 6, 7], it is possible to investigate the internal structure of the corresponding scalar and polarized vector mesons of the models [1, 2, 3] by using the gauge/string duality at large N and strong coupling. This is very interesting because in references [4, 5, 6, 7] it has been found that the behavior of the corresponding structure functions is *model independent* in the sense that relations of the Callan-Gross type, as well as generalizations of it to other structure functions for polarized vector mesons, hold independently of which Dp-brane model one considers. This means that there is a sort of universal behavior for the meson structure functions which should be shared by the large N limit of QCD. This universal property is due to the fact that the dynamics of mesons in the string theory dual model is accounted for by the Dirac-Born-Infeld

(DBI) action of the corresponding flavor Dp-brane. We have chosen the D3D7-brane model for several reasons. Firstly, as we have already mentioned their meson structure functions display universal behavior for relations of the Callan-Gross type. Secondly, the relative simplicity of the geometry of this background allows one to perform a detailed analysis and obtain explicit expressions of the structure functions of scalar mesons in the $1/N$ expansion, which in the end permits to obtain results to compare with lattice QCD and phenomenology. Thirdly, the D3D7-model is the one which compares better with lattice QCD results for the pion and the rho meson (for $N \rightarrow \infty$) [8, 9, 10, 7]. In addition, the fall-off of the structure functions obtained from the D3D7-brane model at large N for $x \rightarrow 1$ leads to a factor $(1-x)^2$, in agreement with phenomenological results [11, 12, 13, 14, 15, 16, 17, 7].

Also, it is interesting to notice that by using the gauge/gravity duality in the case of the $SU(N)$ $\mathcal{N} = 4$ SYM theory glueballs have been studied in the large N limit, while lattice gauge theory simulations have permitted to investigate their properties at finite N [18, 19, 20]. Moreover, meson spectrum and decay constants have been obtained in the quenched approximation with the Wilson fermion action for $N = 2, 3, 4, 5, 6, 7$ and 17 and then extrapolated to $N \rightarrow \infty$ [21, 22].

Recently, the structure of holographic mesons in the [1, 2, 3] models has been investigated in the large N limit and at strong coupling [4, 5, 6, 7], which corresponds to considering single-hadron final states. The process under investigation is the deep inelastic scattering (DIS) of a charged lepton from a hadron. Its differential cross section is obtained in terms of the forward Compton scattering (FCS) by using the optical theorem in quantum field theory (QFT). In the strong coupling limit of the QFT, the appropriate framework to calculate the structure functions is the gauge/string duality [23]. In particular, within the Bjorken parameter range $1/\sqrt{\lambda} \ll x < 1$ for scalar mesons it turns out that the structure function F_1 vanishes since it is proportional to the corresponding Casimir operator of the Lorentz group, which has been confirmed by direct calculation using supergravity [4, 5]. On the other hand, for $\exp(-\sqrt{\lambda}) \ll x \ll 1/\sqrt{\lambda}$, F_1 does not vanish and it is obtained in terms of superstring theory [6]. Recall that λ is the 't Hooft coupling and x the Bjorken parameter. The reason for this behavior of F_1 comes from the fact that at strong coupling the virtual photon probes the entire hadron, thus within the supergravity framework no partons are found in this limit, $1 \ll \lambda \ll N$. The non-vanishing structure function F_2 , on the other hand, has also been calculated in [4, 5, 6] in the corresponding parametric regimes of x , and it has been shown how its first moments agree with the corresponding results from lattice QCD simulations [8, 9, 10] with an accuracy of 10.8% [7]. Similar results have been obtained for the Sakai-Sugimoto model and for the D4D6-brane model [7]. The result of [7] strictly corresponds to the tree-level Feynman diagram for FCS, i.e. by considering a single-hadron final state DIS, which in terms of the following discussion corresponds to considering first the $N \rightarrow \infty$ limit and then the high energy limit.

Beyond the large N limit, within the gauge/string duality framework one must consider the

$1/N$ expansion for which there are two possible approaches which work for different regimes of the Bjorken parameter. For $\exp(-\sqrt{\lambda}) \ll x < 1/\sqrt{\lambda}$ it is required a genus expansion in superstring theory, while for $1/\sqrt{\lambda} \ll x \leq 1$ it is enough to include Feynman loop diagrams in the supergravity calculation. In both situations, a genus-one world-sheet in superstring theory and the corresponding one-loop diagrams in supergravity, lead to the holographic dual description of one-loop FCS in the dual QFT. This corresponds to a two-hadron final state in DIS within two different kinematical regimes of x . Specifically, we can look at the longitudinal structure function of a scalar meson in the $1/N$ expansion, and simultaneously we can also perform an expansion in inverse powers of the momentum transfer of the virtual photon q , which leads to

$$\begin{aligned}
F_L &= F_2 - 2x F_1 \\
&= f_2^{(0)} \left(\frac{\Lambda^2}{q^2} \right)^{\Delta_{in}-1} + \frac{1}{N} \left(f_2^{(1)} - 2x f_1^{(1)} \right) \left(\frac{\Lambda^2}{q^2} \right) + \frac{1}{N^2} \left(f_2^{(2)} - 2x f_1^{(2)} \right) \left(\frac{\Lambda^2}{q^2} \right) + \dots
\end{aligned} \tag{1}$$

where Λ is an IR confining scale of the QFT. Notice that Δ_{in} is the conformal dimension of the incident scalar state in supergravity, while $f_i^{(n)}$'s stand for the structure functions at the corresponding order in $1/N^n$, with $i = 1, 2$ and $n = 0, 1, \dots$, where n indicates the number of loops of the FCS Feynman diagram (i.e. the number of hadrons in the final state DIS).

Recall that for glueballs there is a $1/N^{2n}$ expansion instead of the $1/N^n$ one shown in the previous equation, which simply reflects the fact that glueballs in the calculations [24] are made of $\mathcal{N} = 4$ SYM theory fields in the gauge supermultiplet (thus all of them belong to the adjoint representation of $SU(N)$). On the other hand, the mesons considered here correspond to fields of the hypermultiplet of $\mathcal{N} = 2$ SYM theory, thus being in the fundamental representation. For the glueballs of $\mathcal{N} = 4$ SYM theory it turns out that the large N limit and the high energy limit, i.e. $q^2 \gg \Lambda^2$ do not commute [25, 24]. This leads to an important consequence on the longitudinal structure function for glueballs $F_L^{glueball}$, which shows a rich structure for the currents which contain spin-1, spin-1/2 and spin-0 fields from the $\mathcal{N} = 4$ SYM theory.

We would naively expect that the results for scalar mesons should not change substantially in comparison with those for glueballs. Still it is really worth to carry out these explicit calculations because there are both lattice QCD [8, 9, 10] as well as phenomenological results [11, 12, 13, 14] to compare with for scalar mesons, in particular for the pion.

In fact, we will show how by considering first the high energy limit $q^2 \gg \Lambda^2$ and then the $N \rightarrow \infty$ limit, we obtain expressions for the structure functions for scalar mesons which lead to results for the moments of F_2 which compare very well with lattice QCD simulations⁴. In

⁴Notice that for the comparison with lattice QCD data we consider $F_L \sim F_2$ since F_1 is sub-leading in the large energy limit.

particular, for the case of the pion the agreement with lattice QCD results for the first three moments of F_2 [8, 9, 10] is within 1.27% accuracy. This shows the importance of taking these limits in the correct order to obtain physically sensible results. The reason for the difference between 10.8% accuracy obtained in [7] and the 1.27% accuracy obtained in the present work comes from the fact that in [7] we considered the large N limit first, which implies that in the previous equation only the first term contributes to the structure functions. On the other hand, when we consider first the high energy limit, the second term of equation (1) is the relevant one, while the first term leads to a smaller contribution. In order to have an idea of the level of accuracy of the present results notice for instance that within the gauge/gravity duality two-point functions usually lead to 10% differences with respect to observables for mesons [26, 27], while four-point functions lead to about 30% differences [28, 29], which is reasonable taking into account that these calculations have been done in the large N limit, in comparison with real QCD, i.e. $N = 3$.

Also, it is worth mentioning that for the $\mathcal{N} = 4$ SYM plasma the DC electrical conductivity, spectral functions and photoemission rates are also calculated from the correlation functions of two electromagnetic currents. In fact, these properties have been calculated in [30] in the strong coupling limit for $1 \ll \lambda \ll N$, while in [31, 32, 33, 34] the $\mathcal{O}(\alpha'^3)$ corrections from type IIB superstring theory have been calculated. Although these calculations strictly hold in the large N limit and the strong coupling expansion, i.e. $1/\lambda$, it turns out that by setting $N = 3$ and $\lambda \approx 15$ there is a good agreement with lattice QCD simulations [35]. In addition, for the $\mathcal{N} = 4$ SYM plasma at strong coupling the structure functions F_1 and F_2 have been obtained in [36, 37], while $\mathcal{O}(\alpha'^3)$ corrections from type IIB string theory have been calculated in [38].

This paper is organized as follows. In Section 2 we carry out a detailed derivation of the interaction Lagrangian at different orders in terms of the D7-brane fluctuations. This is done by starting from the Dirac-Born-Infeld action of the D7-brane in the probe approximation. We also describe the solutions of the corresponding equations of motion. In Section 3 we calculate the leading one-loop Feynman-Witten diagram in type IIB supergravity, which corresponds to the Bjorken parameter range $1/\sqrt{\lambda} \ll x < 1$. Then, from this one-loop supergravity diagram we obtain the structure functions for scalar mesons. In Section 4 we perform a comparison with lattice QCD simulations and with phenomenological results, and carry out the discussion and conclusions. Some details of the calculations are described in the appendices.

2 The interaction Lagrangian

2.1 Derivation of the interaction Lagrangian from the D7-brane DBI-action

In this section we begin with the derivation of the interaction Lagrangian corresponding to scalar mesons from the Dirac-Born-Infeld action of a single D7-brane⁵ in the $\text{AdS}_5 \times S^5$ background obtained from the backreaction of N D3-branes in type IIB superstring theory

$$ds^2 = \frac{r^2}{R^2} ds^2(E^{(1,3)}) + \frac{R^2}{r^2} d\vec{Z} \cdot d\vec{Z}. \quad (2)$$

Let us call the metric (2) G_{AB} , with $A, B = 0, 1, \dots, 9$. The Dirac-Born-Infeld action of the D7-brane is given by

$$S = -\mu_7 \int d^8\xi \sqrt{-\det(P[G]_{ab} + 2\pi\alpha' F_{ab})} + \frac{(2\pi\alpha')^2}{2} \mu_7 \int P[C^{(4)}] \wedge F \wedge F, \quad (3)$$

where the relevant part of the Ramond-Ramond potential $C^{(4)}$ is given in [1], while P stands for the pullback of the metric

$$P[G]_{ab} = G_{AB} \frac{dx^A}{d\xi^a} \frac{dx^B}{d\xi^b}, \quad (4)$$

being $a, b = 0, 1, \dots, 7$ the indices which parameterize the D7-brane coordinates. The coordinates perpendicular to the D7-brane are Z^5 and Z^6 , and following [1] one can parameterize the transversal fluctuations in terms of two scalar fields χ and ϕ by

$$Z^5 = 2\pi\alpha'\chi, \quad Z^6 = L + 2\pi\alpha'\phi, \quad (5)$$

which represent the holographic scalar mesons. On the other hand, Z^i with $i = 1, \dots, 4$ are parameterized in terms of spherical coordinates with radius ρ and angles ψ , θ and ω . The radial coordinate r of the AdS_5 can be written in terms of the new coordinates as

$$r^2 = \rho^2 + (L + 2\pi\alpha'\phi)^2 + (2\pi\alpha'\chi)^2, \quad (6)$$

and the metric induced by the D7-brane fluctuations is then

$$ds^2 = \frac{r^2}{R^2} ds^2(E^{(1,3)}) + \frac{R^2}{r^2} [(2\pi\alpha')^2 (d\chi^2 + d\phi^2) + d\rho^2 + \rho^2 d\Omega_3]. \quad (7)$$

In order to solve the equations of motion (EOM) we consider the static gauge with $x^i = \xi^i$ for $i = 0, \dots, 3$, while $\rho = \xi^4$, $\psi = \xi^5$, $\theta = \xi^6$ and $\omega = \xi^7$. Therefore, the holographic scalar

⁵We consider a single-flavor calculation in the dual gauge field theory. The multi-flavor generalization can be easily done following [5], where a single-hadron final state has been considered.

mesons are functions of these coordinates: $\phi(\xi_i)$ and $\chi(\xi_i)$. Moreover, in order to obtain the interaction vertices one has to carry out a Taylor series expansion in ϕ and χ around the classical solution $\phi = 0$ and $\chi = 0$. We identify two kinds of fluctuations of the pullback

$$P[G]_{ab} = \left(G_{MN}|_{\chi, \phi=0} + \frac{\partial G_{MN}}{\partial \chi}|_{\chi, \phi=0} \chi + \frac{\partial G_{MN}}{\partial \phi}|_{\chi, \phi=0} \phi + \mathcal{O}(\phi^2, \phi\chi, \chi^2) \right) \times \left(\delta_a^M \delta_b^N + \delta_8^M \delta_8^N \partial_a \phi \partial_b \phi + \delta_9^M \delta_9^N \partial_a \chi \partial_b \chi \right). \quad (8)$$

Recall that the zeroth order term, $P[G]_{ab}^{(0)}$, is given by $g_{ab} \equiv G_{MN}|_{\chi, \phi=0} \delta_a^M \delta_b^N$, and it is obtained from the induced metric on the D7-brane

$$ds^2 = \frac{r_0^2}{R^2} \eta_{\mu\nu} dx^\mu dx^\nu + \frac{R^2}{r_0^2} \left(d\rho^2 + \rho^2 d\Omega_3^2 \right), \quad (9)$$

where $\mu, \nu = 0, 1, 2, 3$, and $r_0^2 = \rho^2 + L^2$. Thus, due to fluctuations perpendicular to the D7-brane the pullback changes as $P[G]_{ab}^{(0)} \rightarrow P[G]_{ab} = P[G]_{ab}^{(0)} + h_{ab} + X_{ab}$. We can write $h_{ab} = \sum_i h_{ab}^{(i)}$, with $i = 1, \dots, 4$ indicating at which order the scalar fluctuations appear in the metric. Fluctuations h_{ab} come from the $\delta_a^M \delta_b^N$ terms in equation (8). In addition, we must consider the contributions due to the product of the metric expansion times the derivatives of the scalar fluctuations. These generate the kinetic terms of the effective Lagrangian. They are also induced by the perturbations in the transverse directions to the D7-brane and are denoted by $X_{ab} = \sum_j X_{ab}^{(j)}$ with $j = 2, 3, 4$ being j the order at which the fluctuation appears.

In order to calculate h_{ab} and X_{ab} , let us focus on the fluctuations of metric tensor. We only need to consider the following metric warp factors:

$$\frac{r^2}{R^2} = \frac{r_0^2}{R^2} + \frac{1}{R^2} \left[2(2\pi\alpha')L\phi + (2\pi\alpha')^2(\phi^2 + \chi^2) \right] \quad (10)$$

$$\begin{aligned} \frac{R^2}{r^2} &= \frac{R^2}{r_0^2} + \frac{R^2}{r_0^4} \left\{ -2(2\pi\alpha')L\phi + (2\pi\alpha')^2 \left[\left(4\frac{L^2}{r_0^2} - 1 \right) \phi^2 - \chi^2 \right] \right. \\ &\quad \left. + \frac{(2\pi\alpha')^3}{r_0^2} 4L \left[\left(1 - 2\frac{L^2}{r_0^2} \right) \phi^3 + \phi\chi^2 \right] \right\} + \mathcal{O}(\phi^4, \phi^3\chi, \dots). \end{aligned} \quad (11)$$

The expansion is written up to fourth order terms indicated by \mathcal{O} . By plugging these expressions in the induced metric (7) we obtain the h_{ab} and the X_{ab} contributions. The latter are given by

$$X_{ab} = (2\pi\alpha')^2 \left[\frac{R^2}{r_0^2} + \frac{R^2}{r_0^4} \left\{ -2(2\pi\alpha')L\phi + (2\pi\alpha')^2 \left[\left(4\frac{L^2}{r_0^2} - 1 \right) \phi^2 - \chi^2 \right] \right\} \right] \times (\partial_a \phi \partial_b \phi + \partial_a \chi \partial_b \chi) \equiv X_{ab}^{(2)} + X_{ab}^{(3)} + X_{ab}^{(4)}. \quad (12)$$

Now, let us consider a generic background metric M_{ab} with perturbations of the form m_{ab} . One can write the following expression

$$\sqrt{\det(M_{ab} + m_{ab})} = \sqrt{M} \left[1 + \frac{1}{2} m + \left(\frac{1}{8} m^2 - \frac{1}{4} m \cdot m \right) \right]$$

$$\begin{aligned}
& + \left(\frac{1}{48}m^3 - \frac{1}{8}m(m \cdot m) + \frac{1}{6}m \cdot m \cdot m \right) \\
& + \left(\frac{1}{384}m^4 + \frac{1}{32}(m \cdot m)^2 - \frac{1}{32}m^2(m \cdot m) + \frac{1}{12}m(m \cdot m \cdot m) \right. \\
& \left. - \frac{1}{8}m \cdot m \cdot m \cdot m \right) \Big], \tag{13}
\end{aligned}$$

where all indices are raised and lowered with the unperturbed metric M . We use the following notation:

$$m \equiv m_a^a = M^{ab}m_{ab}, \quad m^2 = (M^{ab}m_{ab})^2, \quad m \cdot m \equiv m_b^a m_a^b = M^{bc}M^{ad}m_{ab}m_{cd}. \tag{14}$$

In the present case we set $M_{ab} = g_{ab}$, i.e. the unperturbed metric induced on the D7-brane, and consider the following matrix perturbation $m_{ab} = h_{ab} + X_{ab} + \tilde{F}_{ab}$, where $\tilde{F}_{ab} = 2\pi\alpha'F_{ab}$. Recall that F_{ab} are the contributions from the fluctuations along the D7-brane directions associated with vector mesons.

Now, we can derive the Lagrangian terms order by order in the perturbations as follows.

First order effective Lagrangian

As expected, there are no linear terms in the fluctuations of the metric, thus this Lagrangian vanishes as shown below⁶

$$L_1 = -\mu_7\sqrt{-g} \left[\frac{1}{2}m^{(1)} \right] = -\frac{\mu_7}{2}\sqrt{-g} g^{ab} (h_{ab}^{(1)} + \tilde{F}_{ab}) = -\frac{\mu_7}{2}\sqrt{-g} h^{(1)} = 0, \tag{15}$$

where obviously $g^{ab}\tilde{F}_{ab} = 0$, while the trace of $h^{(1)}$ also vanishes.

Second order effective Lagrangian

This leads to the kinetic terms for the scalar and vector fluctuations which correspond to the kinetic terms of the holographic scalar and vector mesons as in [1],

$$\begin{aligned}
L_2 &= -\mu_7\sqrt{-g} \left[\frac{1}{2}m^{(2)} - \frac{1}{4}m^{(1)} \cdot m^{(1)} + \frac{1}{8}(m^{(1)})^2 \right] \\
&= -\mu_7\sqrt{-g} \left[\frac{1}{2}(h^{(2)} + X^{(2)}) - \frac{1}{4}(\tilde{F} \cdot \tilde{F} + h^{(1)} \cdot h^{(1)} + h^{(1)} \cdot \tilde{F}) + \frac{1}{8}((h^{(1)})^2 + \tilde{F}^2 + h^{(1)}\tilde{F}) \right] \\
&= -\mu_7\sqrt{-g} \left[\frac{1}{2}X^{(2)} + \frac{1}{4}\tilde{F} \cdot \tilde{F} \right] \\
&= -\mu_7(2\pi\alpha')^2\sqrt{-g} \left[\frac{1}{2} \frac{R^2}{\rho^2 + L^2} g^{ab} (\partial_a\phi\partial_b\phi + \partial_a\chi\partial_b\chi) - \frac{1}{4}F_{ab}F^{ab} \right]. \tag{16}
\end{aligned}$$

⁶Note that $X_{ab}^{(1)} = 0$.

Note that there are several vanishing terms due to the antisymmetric character of F_{ab} , and in addition the sum of all terms coming exclusively from h_{ab} at any order in the scalar fluctuations vanishes.

Third order effective Lagrangian

The non-vanishing terms are

$$L_3 = -\mu_7 \sqrt{-g} \left[\frac{1}{2} (X^{(3)} - h^{(1)} \cdot X^{(2)}) + \frac{1}{2} h^{(1)} \cdot \tilde{F} \cdot \tilde{F} \right], \quad (17)$$

which after looking for the explicit dependence of the scalar fluctuations becomes

$$L_3 = -\mu_7 (2\pi\alpha')^3 \sqrt{-g} \left[\frac{R^4 L}{(\rho^2 + L^2)^3} \phi (\partial_\mu \phi \partial_\nu \phi + \partial_\mu \chi \partial_\nu \chi) \eta^{\mu\nu} + \frac{L}{\rho^2 + L^2} \phi (F_{aI} F^{aI} - F_{a\mu} F^{a\mu}) \right], \quad (18)$$

as reported in [1].

Fourth order effective Lagrangian

The fourth order Lagrangian is

$$\begin{aligned} L_4 = & -\mu_7 \sqrt{-g} \left[\frac{1}{2} X^{(4)} + \frac{1}{8} (X^{(2)})^2 - \frac{1}{4} X^{(2)} \cdot X^{(2)} + \frac{1}{32} (\tilde{F} \cdot \tilde{F})^2 - \frac{1}{8} \tilde{F} \cdot \tilde{F} \cdot \tilde{F} \cdot \tilde{F} \right. \\ & - \frac{1}{2} h^{(2)} \cdot X^{(2)} + \frac{1}{2} h^{(1)} \cdot h^{(1)} \cdot X^{(2)} + \frac{1}{2} \tilde{F} \cdot \tilde{F} \cdot X^{(2)} - \frac{1}{8} X^{(2)} (\tilde{F} \cdot \tilde{F}) \\ & - \frac{1}{2} h^{(1)} \cdot X^{(3)} + h^{(1)} \cdot X^{(2)} \cdot \tilde{F} + \frac{1}{2} h^{(2)} \cdot \tilde{F} \cdot \tilde{F} - \frac{1}{2} h^{(1)} \cdot h^{(1)} \cdot \tilde{F} \cdot \tilde{F} \\ & \left. - \frac{1}{4} h^{(1)} \cdot \tilde{F} \cdot h^{(1)} \cdot \tilde{F} \right]. \end{aligned} \quad (19)$$

While these vertices could appear in different one-loop diagrams the related amplitudes turn out to be sub-leading in the high energy limit. Thus, it is not necessary to write down the explicit form of this Lagrangian in terms of the meson fields.

All these are terms of the Lagrangian which are obtained by considering scalar and vector fluctuations on the D7-brane contributing to the one-loop Feynman-Witten diagrams on the gravity side of the calculations.

Effective interaction Lagrangian for gravitons propagating on the D7-brane

In addition to the effective interaction Lagrangian due to transversal and longitudinal fluctuations of the D7-brane, there are also tensor fluctuations of the induced metric on the D7-brane, g_{ab} . They are obtained by considering small perturbations H_{ab} corresponding to gravitons propagating within the D7-brane worldvolume. The effect of this type of tensor fluctuations is reflected both on the squared root of the determinant of the metric, as well as, on the metric used to raise indices on the D7-brane directions. These perturbations couple to fluctuations on the D7-brane. We can consider the fluctuations of the metric of the form $G_{MN} + H_{MN}(x^\mu)$ leading to extra contributions to the pullback $\delta P[G]^H$ due to the ten-dimensional bulk metric fluctuations H_{MN} ,

$$\begin{aligned} \delta P[G]_{ab}^H &= \sum_{i=1}^3 H_{ab}^{(i)} = H_{ab} + H_{a8}(2\pi\alpha')\partial_b\phi + H_{8b}(2\pi\alpha')\partial_a\phi + H_{a9}(2\pi\alpha')\partial_b\chi \\ &\quad + H_{9b}(2\pi\alpha')\partial_a\chi + H_{89}(2\pi\alpha')^2\partial_a\phi\partial_b\chi. \end{aligned} \quad (20)$$

Note that these contributions only include a single graviton. Thus, cubic vertices having a single graviton come from the following Lagrangian

$$\begin{aligned} L_{graviton} &= -\mu_7\sqrt{-g} \left[\frac{1}{2}H^{(3)} - \frac{1}{2}H^{(2)} \cdot h^{(1)} - \frac{1}{2}H^{(1)} \cdot h^{(2)} + \frac{1}{2}H^{(1)} \cdot h^{(1)} \cdot h^{(1)} + \frac{1}{4}H^{(1)}X^{(2)} \right. \\ &\quad \left. - \frac{1}{2}H^{(1)} \cdot X^{(2)} + \frac{1}{2}H^{(1)} \cdot \tilde{F} \cdot \tilde{F} - \frac{1}{8}H^{(1)}(\tilde{F} \cdot \tilde{F}) \right]. \end{aligned} \quad (21)$$

By using the DIS *Ansatz* for the graviton $H_{mi} \sim A_m v_i$, where A_m is a five-dimensional gauge field on AdS_5 while v_i is a Killing vector of S^3 , all terms containing $H_{ab}^{(2)}$ and $H_{ab}^{(3)}$ vanish. Similarly, the trace of $H^{(1)}$ is zero. Also terms like $H^{(1)} \cdot h^{(2)}$ and $H^{(1)} \cdot h^{(1)} \cdot h^{(1)}$ vanish because $h_{ab}^{(i)}$ and g^{ab} are diagonal. Therefore, the above Lagrangian becomes

$$L_{graviton} = -\mu_7\sqrt{-g} \left[-\frac{1}{2}H^{(1)} \cdot X^{(2)} + \frac{1}{2}H^{(1)} \cdot \tilde{F} \cdot \tilde{F} \right]. \quad (22)$$

In principle, we have quartic vertices⁷ which contain a gravi-photon and three mesons. They have the same contribution in powers of N that the diagram with two cubic vertices (one of them contains the graviton)⁸. We do not write them explicitly because these diagrams produce sub-leading contributions in powers of Λ^2/q^2 and will be more suppressed as in [24].

2.2 Solutions of the equations of motion

The equations of motion of the mesons are obtained from the second order fluctuations calculated in last subsection. For scalar mesons, the quadratic Lagrangian is given by $X_{ab}^{(2)}$

⁷These vertices come from $H^{(1)} \cdot X^{(3)}$ or $H^{(1)} \cdot h^{(1)} \cdot X^{(2)}$.

⁸See Subsection 3.2.

and the EOM is

$$\partial_a \left(\frac{\rho^3 \sqrt{-g}}{\rho^2 + L^2} g^{ab} \partial_b \phi \right) = 0 . \quad (23)$$

The solutions have been calculated in terms of Hypergeometric functions in [1]. $L \sim \Lambda R^2$ plays the role of a cut-off in the radial coordinate. In the limit $L \rightarrow 0$ the conformal symmetry is recovered, the coordinate $\rho \rightarrow r$ and the induced metric becomes $AdS_5 \times S^3$.

We are interested in the high energy limit, $q^2 \gg \Lambda^2$, therefore we shall consider finite but small values of L such that the background is approximately $AdS_5 \times S^3$ and the solutions are somehow similar to those for glueballs in $AdS_5 \times S^5$. This allows one to have cubic vertices which are linearly proportional to L , and use the solutions of meson fields obtained in [4]. By solving the EOM in the limit $\rho \gg L$ and by imposing a hard cut-off, we obtain the solutions for the scalar fields $\Phi = \phi, \chi$ with some four-momentum k^μ as

$$\Phi^{(l)}(x^\mu, z, \Omega) = c e^{ik \cdot x} z J_{\Delta-2}(kz) Y^l(\Omega) , \quad (24)$$

where we have introduced the variable $z = R^2/\rho$ and a normalization constant $c \sim \sqrt{\Lambda k}$, while $Y^l(\Omega)$ is a scalar spherical harmonic on S^3 . Notice that for closed strings there is a factor z^2 instead of z multiplying the Bessel function J . The EOM for the gauge fields ($F_{ab} = \partial_a B_b - \partial_b B_a$) on the D7-brane which follows from the second term in (16) plus the Wess-Zumino term, is

$$\partial_a \left(\sqrt{-g} F^{ab} \right) - \frac{4\rho(\rho^2 + L^2)}{R^4} \epsilon^{bjk} \partial_j B_k = 0 , \quad (25)$$

where ϵ_{ijk} is the Levi-Civita pseudo-tensor density, the indices a, b, c, \dots run over all directions of the D7-brane world-volume, and i, j, k, \dots belong to S^3 . The second term is the contribution from the Wess-Zumino action and it is nonzero only if b is one of the S^3 indices. We can expand B_M in scalar and vector spherical harmonics on S^3 , and obtain three modes

$$\text{type I} \quad : \quad B_\mu = 0, \quad B_\rho = 0, \quad B_i = \phi_I^\pm(\rho) e^{ik \cdot x} Y_i^{l, \pm 1}(\Omega), \quad (26)$$

$$\text{type II} \quad : \quad B_\mu = \zeta_\mu \phi_{II}(\rho) e^{ik \cdot x} Y^l(\Omega), \quad k \cdot \zeta = 0, \quad B_\rho = 0, \quad B_i = 0, \quad (27)$$

$$\text{type III} \quad : \quad B_\mu = 0, \quad B_\rho = \phi_{III}(\rho) e^{ik \cdot x} Y^l(\Omega), \quad B_i = \tilde{\phi}_{III}(\rho) e^{ik \cdot x} \nabla_i Y^l(\Omega). \quad (28)$$

$Y_i^{l, \pm 1}(\Omega)$ and $\nabla_i Y^l(\Omega)$ are the different vector spherical harmonics on S^3 . The solutions are associated with different representations of the isometry group of $SO(4) \approx SU(2) \times SU(2)$. The properties of the modes and their on-shell solutions are shown in table 1. For type I and III modes, which interact with the scalar meson, we obtain the following ρ dependence

Field	Type of field in 5D	Built from	$\Delta(l)$	$SU(2) \times SU(2)$ irrep
ϕ, χ	scalars	ϕ, χ	$l + 3, l \geq 0$	$(\frac{l}{2}, \frac{l}{2})$
B_μ	vector	B_μ^{II}	$l + 3, l \geq 0$	$(\frac{l}{2}, \frac{l}{2})$
ϕ_I^-	scalar	B_i^I	$l + 1, l \geq 1$	$(\frac{l+1}{2}, \frac{l-1}{2})$
ϕ_I^+	scalar	B_i^I	$l + 5, l \geq 1$	$(\frac{l-1}{2}, \frac{l+1}{2})$
ϕ_{III}	scalar	$B_{i,z}^{III}$	$l + 3, l \geq 1$	$(\frac{l}{2}, \frac{l}{2})$

Table 1: Some features of D7-brane fluctuations around the $\text{AdS}_5 \times S^3$ background which are relevant to this work. The integer l indicates the $SO(4) \sim SU(2) \times SU(2)$ irreducible representation (irrep) and defines the corresponding Kaluza-Klein mass. The relation between the scaling dimension of the associated operator Δ and l is written.

(in the limit $q^2 \gg \Lambda^2$)

$$\phi_I^{\pm 1}(\rho) = c_I \frac{J_{\Delta-2}(\frac{MR^2}{\rho})}{\rho^2}, \quad \phi_{III}(\rho) = c_{III} \frac{J_{\Delta-2}(\frac{MR^2}{\rho})}{\rho^2}, \quad \tilde{\phi}_{III}(\rho) = \frac{\frac{1}{\rho} \partial_\rho (\rho^3 \phi_{III}(\rho))}{l(l+2)}, \quad (29)$$

where the constants are $c_I \sim R^4 \sqrt{M\Lambda}$ and $c_{III} \sim R^2 \sqrt{\frac{l(l+2)\Lambda}{M}}$. In this work we use the propagator of the type I mode. Since the solution in the AdS is analogous to the glueball solution, we can use a similar propagator as in references [24, 25]

$$G_\Delta(x, z; x', z') = - \int \frac{d^4 k}{(2\pi)^4} \int \frac{d\omega \omega}{\omega^2 + k^2 - i\epsilon} z^2 J_{\Delta-2}(\omega z) (z')^2 J_{\Delta-2}(\omega z'), \quad (30)$$

together with the corresponding vector spherical harmonics.

Using the gauge/string duality the current operator inserted at the boundary of the AdS excites a non-normalizable mode which propagates within the bulk. The perturbations (gravi-photons) take the form $\delta G_{mi} = A_m v_i$. The field A_m is derived from a Maxwell Lagrangian in the AdS space with the boundary condition $A_\mu(y, \infty) = n_\mu e^{iq \cdot y}$. In the Lorentz-like gauge the solution is given by

$$A_\mu = n_\mu e^{iq \cdot y} q z K_1(q z), \quad A_z = i n \cdot q e^{iq \cdot y} z K_0(q z), \quad (31)$$

where K_0 and K_1 are modified Bessel functions of the second kind.

3 The leading diagram in the $1/N$ expansion

3.1 DIS and comments on the FCS tree-level calculation

The DIS cross section is related to the matrix element of a product of two electromagnetic currents $J_\mu(y) J_\nu(0)$ inside the hadron. Through the so-called optical theorem, one has to calculate the FCS process associated with the DIS one. Specifically, there are two steps to follow. The first one is given by the operator product expansion of $J_\mu(y) J_\nu(0)$, which is obtained within an un-physical region of the Bjorken parameter, $x \gg 1$. For the second step one needs to consider the dispersion relations in order to connect the un-physical calculation with the physical DIS process for $0 \leq x < 1$.

Recall that the matrix element of two electromagnetic currents $J_\mu(y) J_\nu(0)$ inside a hadron can be expressed by using the $T_{\mu\nu}$ tensor. For the incoming and outgoing hadrons with polarizations h and h' , we can write

$$T_{\mu\nu}(q^2, x) = i \int d^4y e^{iq \cdot y} \langle P, h' | \hat{T}(J_\mu(y) J_\nu(0)) | P, h \rangle. \quad (32)$$

By using the optical theorem the $T_{\mu\nu}$ tensor is related to the hadronic tensor $W_{\mu\nu}$ as follows,

$$W_{\mu\nu}(q^2, x) = i \int d^4y e^{iq \cdot y} \langle P, h' | [J_\mu(y), J_\nu(0)] | P, h \rangle. \quad (33)$$

In the present work we investigate scalar mesons, which reduces this tensor to only two terms

$$W_{\mu\nu} = F_1(x, q^2) \left(\eta_{\mu\nu} - \frac{q_\mu q_\nu}{q^2} \right) + \frac{2x}{q^2} F_2(x, q^2) \left(P_\mu + \frac{q_\mu}{2x} \right) \left(P_\nu + \frac{q_\nu}{2x} \right), \quad (34)$$

where it has been used the Bjorken parameter defined as

$$x = \frac{-q^2}{2P \cdot q}, \quad (35)$$

while $F_1(x, q^2)$ and $F_2(x, q^2)$ are the so-called structure functions. At weak coupling these functions are obtained within the parton model, and they are related to the parton distribution functions (PDFs). The PDFs represent the probability of finding a parton with a fraction x of the target hadron momentum, P . Particularly, from the optical theorem one learns that 2π times the imaginary part of the structure functions associated with FCS gives exactly the DIS structure functions. Based on this Polchinski and Strassler [23] proposed a way to calculate structure functions at strong coupling by using the gauge/string theory duality.

The tree-level type IIB supergravity calculation, which in terms of the $1/N$ expansion implies taking the large N limit from the beginning, has been done in [4] and [5]. In the

range $1/\sqrt{\lambda} \ll x < 1$ the results using the D3D7-brane model for scalar mesons have been obtained in [4] for one flavor (and in [5] for the multi-flavor case) obtaining

$$F_1 = 0, \quad F_2 = \tilde{A}_0 \mathcal{Q}^2 \left(\frac{\Lambda^2}{q^2} \right)^{l+2} x^{l+4} (1-x)^{l+1}, \quad (36)$$

where $\tilde{A}_0 = 2^{2l-4} \pi^{-7} (l+2)!^2 |c_i|^2 |c_X|^2$ is a dimensionless normalization constant, while c_i and c_X are the normalization constants of the incident and intermediate (in FCS) scalar mesons. We consider that the integer $l > 0$, which means that the scalar fields are charged under a $U(1)$ group. Notice that \mathcal{Q} labels the charge under the $U(1)$ symmetry group induced by transformations on the three-sphere in the direction of the Killing vector v^j .

On the other hand, although in the present work we only consider the calculation within the validity range of supergravity, we can also write the structure functions for scalar mesons for small x values within the range $\exp(-\sqrt{\lambda}) \ll x \ll 1/\sqrt{\lambda}$. In this case the calculation has been done by considering type IIB string theory scattering amplitudes of two open strings (representing the scalar mesons) and two closed strings (which represent the two virtual photons in the FCS). This has been done in [6], obtaining

$$F_1 = \frac{\pi^2}{16x^2} \rho_3 |c_i|^2 \left(\frac{\Lambda^2}{q^2} \right)^{l+1} \frac{1}{\sqrt{4\pi\lambda}} I_{1,2l+5}, \quad (37)$$

$$F_2 = \frac{\pi^2}{8x} \rho_3 |c_i|^2 \left(\frac{\Lambda^2}{q^2} \right)^{l+1} \frac{1}{\sqrt{4\pi\lambda}} (I_{0,2l+5} + I_{1,2l+5}). \quad (38)$$

Notice that ρ_3 is defined through the normalization condition for the spherical harmonics on S^3

$$\int d\Omega_3 \sqrt{\tilde{g}} v_i v^i Y(\Omega_3) Y^*(\Omega_3) = \rho_3 R^2. \quad (39)$$

Also the definition of $I_{j,n}$ is given in terms of the integral of the square of the modified Bessel functions of the second kind times integer powers of its argument $\omega = \frac{qR^2}{r}$,

$$I_{j,n} = \int_0^\infty d\omega \omega^n K_j^2(\omega). \quad (40)$$

Next we focus on the type IIB supergravity calculation of one-loop diagrams which are the holographic dual representation of the one-loop FCS corresponding to a DIS process with two outgoing hadron states. The following calculations hold in the kinematical range $1/\sqrt{\lambda} \ll x < 1$, and at strong coupling.

3.2 The leading diagram for the one-loop FCS calculation

We can redefine the fields in such a way that their kinetic terms become canonically normalized in terms of N , i.e. they do not depend on N . Through this field redefinition it

is possible perform the $1/N$ counting of each Feynman-Witten diagram. By noting that $\mu_7 = [(2\pi)^7 g_s \alpha'^4]^{-1} = 2N[R^4(2\pi)^6 \alpha'^2]^{-1}$, the scalar and vector meson fields are redefined as

$$\phi \rightarrow \frac{\phi}{\sqrt{N}}, \quad \chi \rightarrow \frac{\chi}{\sqrt{N}}, \quad F_{ab} \rightarrow \frac{F_{ab}}{\sqrt{N}}. \quad (41)$$

Notice that with this field redefinition the cubic and quartic vertices have the factors $1/\sqrt{N}$ and $1/N$, respectively.

In addition, the normalization for the graviton modes (closed strings) implies a different power of N in comparison with the meson fields, since in order to obtain canonically normalized quadratic terms one has to re-scale

$$H_{ab} \rightarrow \frac{H_{ab}}{N}, \quad (42)$$

since the Newton's constant in type IIB supergravity is $1/k_{10}^2 = N^2/(4\pi^5 R^8)$.

The arguments used to select the leading diagram contributing to the $1/N$ expansion are similar to those exposed in [24] and [25]. The idea is to understand what changes when considering large but finite values of the number of color degrees of freedom in the holographic calculation of the structure functions $F_i(x, q^2)$ of scalar mesons obtained from the D3D7-brane model, with respect to the methods and results of the tree-level calculation performed in [4, 5]. Moreover, we want to compare both the results of the present $1/N$ expansion and those of [4, 5, 7] in the large N limit with lattice QCD simulations for the first three moments of the F_2 structure function of the pion [8, 9, 10]. Since we focus on the $1/\sqrt{\lambda} \ll x < 1$ range the supergravity description is accurate enough. Therefore, in order to obtain the leading $1/N$ correction⁹ we have to consider all one-loop diagrams that can be drawn for the holographic dual FCS process. This involves two non-normalizable gauge bosons A_μ coming from the boundary, plus two normalizable modes on the D7-brane, in this case the scalar mesons that describe the D7-brane transverse fluctuations. By using the optical theorem we just need to calculate the imaginary parts of these diagrams, which means that we have to introduce a vertical cut in the one-loop supergravity Feynman-Witten diagrams and, therefore, we have to consider two-particle on-shell intermediate states. All these fields and their interactions have been described in the previous section for small but non-vanishing L . This permits to unveil important physical aspects of the process.

The crucial point is that we are working in the large- q^2 limit. This allows one to classify diagrams in a Λ^2/q^2 series expansion. The q^μ four-moment is carried by a gauge field, which is the holographic dual representation of a virtual photon on the boundary gauge theory. As

⁹In fact, at the end of the calculation, after considering the high energy limit first, it will become clear that the result will not be a correction but the leading contribution. Obviously, if one considers the large N limit first, which in the high energy limit is not the physical situation, it can be seen as a $1/N$ correction, see equation (1).

in the case of the $\text{AdS}_5 \times S^5$ fields, which we carefully studied in [24], the vertices coupling to the A_μ field (which is a five-dimensional field after integrating over the S^3) with scalar bulk fields are always of the same form

$$S_{\Phi\Phi A} \propto \int d^{p+1}x \sqrt{-g} h^{ab} \partial_a \Phi \partial_b \Phi, \quad h^{ab} \sim (A^a v^b + A^b v^a), \quad (43)$$

where Φ represents some generic scalar field. This implies that in the on-shell evaluation of this vertex for a given field Φ_Δ coming from the IR region we will find a suppression factor $(\Lambda^2/q^2)^{\Delta-1}$ in the structure functions. The physical reason for this suppression is understood as follows. Bessel- J functions of bulk fields solutions (incident holographic hadrons) mainly live in the IR region near $z \sim \Lambda^{-1}$, while the Bessel- K function decreases exponentially from the boundary towards the interior. This fall-off is characterized by q , hence the Λ^2/q^2 factor and its Δ power are related with the probability for the Φ_Δ hadron to tunnel from the IR to the UV region where it can interact with the gauge field [23].

We should mention that after studying other types of vertices, such as quartic interactions, and checking that they do not change this analysis, we can conclude that the Λ/q expansion will be dominated by processes where the non-normalizable gauge field interacts with the scalars with the smallest possible value of Δ . In the $N \rightarrow \infty$ limit there is only one allowed interaction vertex, and this index (conformal dimension) is fixed by the incoming hadron with its associated scaling dimension Δ_{in} , but when the number of color degrees of freedom becomes finite one must take into account the one-loop processes where the initial hadron splits into two other particles, and only one of them interacts with A_μ . The leading contribution comes from the case where this splitting happens in IR region. Furthermore, among the fields that one obtains within the D3D7-brane model we can see that the type I gauge fields will play a key role since they can have the lowest $\Delta_{min} = 2$ index. Note that this is the same Δ_{min} that we have obtained in [24] in the $\text{AdS}_5 \times S^5$ context from the scalar fields usually called s -scalars, a particular combination of graviton and 4-form perturbations [39]. Thus, the $1/q^2$ dependence of the final result will be the same as in our paper [24], however the dependence on the Bjorken parameter x will be significantly different.

The conclusion from this analysis is that the fields involved in the calculation and the diagram rendering the leading contribution to the on-shell scattering amplitude and the structure functions of the scalar mesons are given schematically by the diagram of figure 1.

In the following subsection we will analyze explicitly the two interaction vertices and the propagator that appears in this diagram. The interaction vertices are: the IR vertex where the initial hadron splits into two intermediate hadrons, and the UV vertex where one of the resulting fields interacts with the gauge field near the boundary. We will also carry out the final steps of the calculation and, within some approximations, obtain the explicit form of the longitudinal structure function $F_L = F_2 - 2xF_1$.

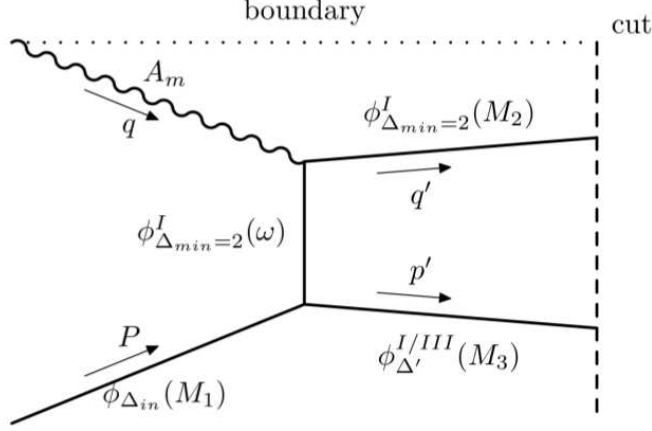


Figure 1: Feynman-Witten diagram corresponding to the left side of the cut (vertical long-dashed line) of the leading one-loop FCS related through the optical theorem to the DIS diagram with a two-hadron final state. The field associated with each line is explicitly written with the corresponding four-dimensional momenta, Δ indices and AdS masses. The solutions are described in Section 2.

3.3 The UV interaction vertex

This vertex comes from the second term in the Lagrangian of equation (22), where the metric fluctuation couples to two vector modes. In principle, both F_{ab} can be built out from one of the vector modes of type I $^\pm$, II or III. The one associated with the vertical propagator in figure 1 must be the type I $^-$ mode, which has the lowest possible index $\Delta_{min} = 2$. The relevant interaction is of the form $A\phi_I\phi_I$. The situation where the second vector involved in the UV interaction vertex is a type II or type III mode is excluded since in that case the interaction Lagrangian vanishes because of the angular integral. The effective action associated with this vertex is

$$S_{A\phi_I\phi_I} = -\frac{\mu_7}{N}(2\pi\alpha')^2 \int d^4x d\rho d\Omega_3 \sqrt{-g} \frac{1}{2} H^{(1)} \cdot F^I \cdot F^{*I} , \quad (44)$$

where

$$F_{\mu\nu}^I = 0 , \quad F_{\mu z}^I = 0 , \quad F_{\mu i}^I = \partial_\mu B_i^I , \quad F_{zi}^I = \partial_z B_i^I , \quad (45)$$

thus, we have

$$\begin{aligned} H^{(1)} \cdot F^I \cdot F^{*I} &= g^{bc} g^{de} g^{af} h_{ab} F_{cd}^I F_{ef}^{*I} \\ &= A^\mu v^i g^{de} F_{\mu d}^I F_{ei}^{*I} + A^\mu v^i g^{de} F_{id}^I F_{e\mu}^{*I} \\ &= A^\mu v^i \partial_\mu B_I^j (\partial_j B_i^{*I} - \partial_i B_j^{*I}) + A^\mu v^i \partial_\mu B_I^{*j} (\partial_j B_i^I - \partial_i B_j^I) \\ &= - \left(A^\mu \partial_\mu B^j v^i \partial_i B_j^* + A^\mu \partial_I B^{*j} v^i \partial_i B_j \right) . \end{aligned} \quad (46)$$

In order to evaluate the on-shell vertex one must insert the actual form of the solutions described in the previous section and integrate over the eight-dimensional space. The integration over the first four coordinates x^μ is trivial since it always renders the momentum conservation condition associated with the corresponding momenta. The integrals over the spherical harmonics can be simplified by considering the charge eigenstates¹⁰

$$v^i \partial_i Y^j = i \mathcal{Q} Y^j . \quad (47)$$

Finally, by changing variables $z = \frac{R^2}{\rho}$, the effective action becomes

$$S_{A\phi_I\phi_I} = i \mathcal{Q} \frac{\mu_7}{N} 2 (\pi\alpha')^2 \int d^4x dz d\Omega_3 \sqrt{-g} A^m(z) \times \\ \left(B^{Ii}(z, \Omega) \partial_m B_i^{*I}(z, \Omega) - B_i^{*I}(z, \Omega) \partial_m B^{Ii}(z, \Omega) \right) . \quad (48)$$

Type I modes labeled with (\pm) are orthogonal and therefore they do not couple to each other. The only outgoing particle is a type I scalar mode with label $(-)$ and with the same quantum numbers with l, m, m' as the incoming scalar. Hence, even if in the full 8-dimensional theory the type I modes come from gauge fields and the existence of their solution rely on the presence of the Wess-Zumino term in the action together with the DBI term in [1] the angular integral only leads to charge conservation, which also indicates that there is no mixing with other particles in this vertex. Then, the on-shell action that we obtain is exactly the same found for glueballs [23], scalar mesons [4, 5] and s scalars [24].

After integration of equation (48) on S^3 , by using the orthogonality relations of the vector spherical harmonics, we obtain

$$S_{A\phi_I\phi_I} = i \mathcal{Q} \frac{\mu_7}{N} 2 (\pi\alpha')^2 \int d^4x dz \sqrt{-g} A^m(z) (\phi_I(z, \Omega) \partial_m \phi_I^*(z) - \phi_I^*(z) \partial_m \phi_I(z)) , \quad (49)$$

where $\phi^I = \sqrt{\Lambda\omega} e^{i(P-p_\omega)\cdot x} z^2 J_{\Delta_\omega-2}(\omega z)$ and $\phi^{I*} = \sqrt{\Lambda M_3} e^{-iq'\cdot x} z^2 J_{\Delta_\omega-2}(M_3 z)$.

3.4 The IR interaction vertex

The relevant vertex couples the incident scalar meson to a scalar mode of type I^- having the smallest conformal dimension $\Delta_{min} = 2$ corresponding to $l = 1$. From the Lagrangian at cubic order the only term which couples the scalar meson ϕ to type I^\pm eight-dimensional vector modes is the second term of equation (17). Thus, for small L we have¹¹

$$L_{\phi FF} = \frac{\mu_7}{N^{3/2}} (2\pi\alpha')^3 \sqrt{-g} \frac{L}{\rho^2} \phi \left(F_{IJ} F^{IJ} - F_{\mu\nu} F^{\mu\nu} \right) . \quad (50)$$

¹⁰Notice that the charge \mathcal{Q} does not need to be the one carried by the initial hadron, \mathcal{Q}_i because of the hadron splitting process.

¹¹Note that in the conformal case, i.e. $L = 0$, this vertex does not exist. Here, we analyze the situation for the non-conformal background and keep a non-vanishing but small L in order to approximate the Hypergeometric functions by Bessel functions. The $L = 0$ case should be analyzed in a different way.

Since one of the vector modes must be of type I^- , its field strength is such that $F_{\mu\nu}^I = 0$. Hence, we are left with the term proportional to $F_{IJ}F^{IJ}$ only. Note that this implies that the on-shell mode produced in this process (whose mass is denoted by M_3) cannot be a type II mode. This means that we only have to consider scalar modes from the five-dimensional point of view. The remaining two-form field strength contraction can be decomposed in terms of angular coordinates on S^3 , and the radial coordinate ρ as

$$F_{IJ}F^{IJ} = F_{ij}F^{ij} + 2F_{i\rho}F^{i\rho} = 2 \left[\nabla_i B_j \nabla^i B^j - \nabla_i B_j \nabla^j B^i + \nabla_\rho B_i \nabla^\rho B^i - \nabla_\rho B_i \nabla^i B^\rho \right], \quad (51)$$

where in the last step we have used the fact that for a type I mode $B_\rho = 0$. Plugging it in the action and taking the complex conjugate field for the outgoing field we obtain

$$\begin{aligned} S_{\phi\phi_I\phi_I} &= -\frac{\mu_7}{N^{3/2}} (2\pi\alpha')^3 \times \\ &\int d^8\xi \sqrt{-g} \frac{2L\phi}{\rho^2} \left(\nabla_i B_j \nabla^i B^{j*} - \nabla_i B_j \nabla^j B^{i*} + \nabla_\rho B_i \nabla^\rho B^{i*} - \nabla_\rho B_i \nabla^i B^{\rho*} \right), \end{aligned} \quad (52)$$

where B corresponds to the type I^- scalar mode with mass ω which comes from the propagator and interacts with the virtual photon in the UV region. On the other hand, B^* is the outgoing mode with mass M_3 . We will analyze in detail the case where this mode is of type I^\pm . The possibility for the on-shell mode outgoing from this IR vertex to be of type III is considered in Appendix B.

If the outgoing normalized mode corresponds to a type I scalar one has $B_\rho^* = 0$ and, therefore, the last term in equation (52) vanishes. Plugging the solutions of the modes in the action and taking into account that $\Delta = \Delta_{min} = 2$ for the scalar that corresponds to the vertical propagating line in the diagram of figure 1 we find the following interaction action,

$$\begin{aligned} S_{\phi\phi_I\phi_I}^{I^\pm} &= -\frac{\mu_7}{N^{3/2}} (2\pi\alpha')^3 2L C \int d^4x e^{i(p_1+p_\omega-p_3)x} \left(\int_0^{\frac{1}{\Lambda}} dz z^2 J_{\Delta_{in}-2}(M_1 z) J_0(\omega z) J_{\Delta_3-2}(M_3 z) I_1 \right. \\ &\quad \left. + \int_0^{\frac{1}{\Lambda}} dz J_{\Delta_{in}-2}(M_1 z) \partial_z(z^2 J_0(\omega z)) \partial_z(z^2 J_{\Delta_3-2}(M_3 z)) I_2 \right), \end{aligned} \quad (53)$$

where Δ_{in} and Δ_3 are associated with the spherical harmonic representation index of the incident and outgoing on-shell modes, respectively, and $C = \sqrt{\Lambda^3 M_1 M_3 \omega}$ is the product of the corresponding normalization constants discussed in Section 2. In addition, I_1 and I_2 are integrals of the spherical harmonics on S^3 defined as follows

$$I_1 = \int d\Omega_3 \left(\nabla_i \vec{Y}^{l''} \cdot \nabla^i \vec{Y}^1 Y^{l_{in}} - \nabla_i Y_j^{l''} \cdot \nabla^j Y^{1,i} Y^{l_{in}} \right), \quad I_2 = \int d\Omega_3 \vec{Y}^{l''} \cdot \vec{Y}^1 Y^{l_{in}}, \quad (54)$$

where l'' and l_{in} are related to the conformal dimensions as shown in table 1. By using properties of vector spherical harmonics we obtain the following identity

$$\pm(l+1)\epsilon_{ilm} Y_i^{l,\pm} = \epsilon_{ilm} \epsilon_{ijk} \nabla_j Y_k^{l,\pm} = \nabla_l Y_m^{l,\pm} - \nabla_m Y_l^{l,\pm}, \quad (55)$$

which allows us to express one of these integrals in terms of the other as

$$I_1 = \int d\Omega_3 Y^{l_{in}} \nabla^i Y^{l'', \pm, j} \left(\nabla_i Y_j^{1, -} - \nabla_j Y_i^{1, -} \right) = \mp 2(l'' + 1) I_2. \quad (56)$$

The result of the integral I_1 is presented in Appendix A and it restricts the conformal dimension of the outgoing mode. In order to calculate the structure functions we have to sum over indices m and n of the spherical harmonics of the intermediate field by using the optical theorem. Note that there are many vanishing terms due to the $U(1)$ charge conservation associated with these indices.

Hitherto we have worked from first principles, finding the leading diagram and studying the needed on-shell vertices and propagators. Once we have dealt with the angular integrals, we are left with definite z -integrals (within the integration region given by $0 \leq z \leq z_0$, where $z = 0$ is the AdS-boundary and $z_0 = \Lambda^{-1}$ corresponds to the IR cut-off) of products of three Bessel functions of the first kind times some positive integer power of z . Since these integrals are not known analytically, there are two ways to proceed. The first one would be a numerical approach, simplified by the fact that since the splitting occurs mainly in the IR region, the Bessel functions can be replaced by their asymptotic expression

$$J_m(az) \approx \sqrt{\frac{2}{\pi az}} \cos\left(az - m\frac{\pi}{2} - \frac{\pi}{4}\right). \quad (57)$$

However, the intricate x -dependence of the scattering amplitude difficults the extraction of the x -dependence of the structure functions. In this work we will proceed as in [24] and attempt to obtain these functions $F_i(x, q^2)$ semi-analytically within the range of validity of some reasonable approximations. Most of the details of the following calculations can be found in our previous work [24], and the new ingredients that appear due to the different structure of the IR vertex are analyzed in this section and are collected in Appendix C.

3.5 Calculation of the structure functions

The $1/N$ corrections to the structure functions can be obtained from the hadronic tensor as in [24] where glueballs have been considered. One focuses on the DIS process in the boundary theory, and isolates the contribution from two-particle intermediate states to the hadronic tensor $W^{\mu\nu}$ in terms of the corresponding electromagnetic current J^μ one-point functions, which is related to the FCS tensor $T^{\mu\nu}$ by the optical theorem. In this context we can schematically write

$$\begin{aligned} \text{Im}(T_2^{\mu\nu}) &= \pi \sum_{X_1, X_2} \langle P, Q | \tilde{J}^\mu(q) | X_1, X_2 \rangle \langle X_1, X_2 | J^\nu(0) | P, Q \rangle \\ &= \pi \sum_{M_2, M_3} \int \frac{d^3 p'}{2E_{p'}(2\pi)^3} \frac{d^3 q'}{2E_{q'}(2\pi)^3} \langle P, Q | \tilde{J}^\mu(q) | X_1, X_2 \rangle \langle X_1, X_2 | J^\nu(0) | P, Q \rangle \end{aligned} \quad (58)$$

$$= 4\pi^3 \sum_{M_2, M_3} \int \frac{d^4 q'}{(2\pi)^4} \delta(M_2^2 - q'^2) \delta(M_3^2 - (P + q - q')^2) |\langle P, Q | J^\nu(0) | X_1, X_2 \rangle|^2,$$

where the subindex in $T_2^{\mu\nu}$ indicates that we are considering only processes with two-particle intermediate states X_1 and X_2 associated with the momenta p' and q' (see figure 1), and

$$n_\mu \langle P, Q | \tilde{J}^\mu(q) | X_1, X_2 \rangle = (2\pi)^4 \delta^{(4)}(P + q - p' - q') \langle P, Q | n \cdot J(0) | X_1, X_2 \rangle, \quad (59)$$

is identified in the AdS/CFT duality with the amplitude of our diagram of figure 1. We refer the reader to our previous paper [24] for details of the rest of the calculation since there are several common steps. As in references [24, 25] the dominant diagram is the t -channel one. Therefore, the tensor structure of the amplitude is governed by¹²

$$v_s^\mu \equiv \frac{1}{q} \left(P^\mu + \frac{q^\mu}{2x} \right) \quad \text{and} \quad v_t^\mu \equiv \frac{1}{q} \left(q'^\mu + \frac{q^\mu}{2y'} \right) \quad \text{with} \quad y' = \frac{-q^2}{2q' \cdot q}, \quad (60)$$

which means that the structure functions are obtained from

$$F_1(x, q^2) = \pi \sum_{M_2, M_3} \int \frac{d^3 p'}{2E_{p'}(2\pi)^3} \frac{d^3 q'}{2E_{q'}(2\pi)^3} (2\pi)^4 \delta^{(4)}(P + q - p' - q') |C_t|^2 \times 2q^2 [v_t^2 + 4x^2(v_s \cdot v_t)^2], \quad (61)$$

$$F_2(x, q^2) = \pi \sum_{M_2, M_3} \int \frac{d^3 p'}{2E_{p'}(2\pi)^3} \frac{d^3 q'}{2E_{q'}(2\pi)^3} (2\pi)^4 \delta^{(4)}(P + q - p' - q') |C_t|^2 \times 4xq^2 [v_t^2 + 12x^2(v_s \cdot v_t)^2], \quad (62)$$

where C_t is given by

$$\begin{aligned} C_t(M_2, M_3, p', q') &= \int dz dz' [V_{IR}(z) \times V_{UV}(z') \times G(z, z')] \\ &= \int d\omega \frac{\omega}{\omega^2 + (P - p')^2} S_{\phi_I \phi_I}^{(z)}(M_1, M_3, \omega) S_{A\phi_I \phi_I}^{(z')}(M_2, q, \omega), \end{aligned} \quad (63)$$

where the momentum conservation Dirac delta functions have been written in equations (61) and (62). This means that we can identify a first term in the F_i functions that fulfills exactly the Callan-Gross relation $F_2 = 2xF_1$, and a second term which contributes to the longitudinal structure function

$$\begin{pmatrix} F_1 \\ F_2 \\ F_L \end{pmatrix} = \frac{1}{N} \sum_{M_2 M_3} \frac{q|\vec{p}'|}{8} \sqrt{\frac{x}{1-x}} \int d\theta \sin \theta \begin{pmatrix} v_t^2 + 4x^2(v_s \cdot v_t)^2 \\ 2x[v_t^2 + 12x^2(v_s \cdot v_t)^2] \\ 16x^3(v_s \cdot v_t)^2 \end{pmatrix} |C_t|^2. \quad (64)$$

¹²Note that y' plays the role of the Bjorken parameter for the scattering of the scalar ϕ_I mode and the gauge field A^μ .

One should keep in mind that the N^{-1} pre-factor carries all the dependence on the number of colors once the fields have been re-scaled in order to obtain canonically normalized kinetic term in the Lagrangian. The term corresponding to F_1 turns out to be sub-leading in the large- q^2 expansion, thus we focus on the calculation of $F_L(x, q^2)$. The constant C_t contains the integrals in z of each vertex as well as the contribution from the propagator of type I scalars $G(z, z')$, which has the same form as in the case of glueballs.

The main difference with respect to the glueball case of [24] comes from the integrals of the IR interaction vertex, containing integrals of three Bessel functions of the first kind multiplied by z^κ , with positive integer values κ . Recall that the $\kappa = 1$ case appears for the glueballs. In the present case, although the z -integrals are difficult to be solved analytically, due to the presence of the cut-off $z_0 = \Lambda^{-1}$ we can approximately relate them to the one with $\kappa = 1$ and then analyze them by using techniques inspired in the case studied by Auluck [41]. These approximations are described in detail in Appendix C. The resulting formulas that will be used in the rest of this section in order to obtain the structure functions are given by the equations

$$\begin{aligned} I^{(\kappa)}(a, b, c, \Lambda) &\equiv \int_0^{\Lambda^{-1}} dz z^\kappa J_m(az) J_n(bz) J_l(cz) \\ \Rightarrow \Lambda^3 I^{(4)}(a, b, c, \Lambda) &\approx \Lambda^2 I^{(3)}(a, b, c, \Lambda) \approx \Lambda I^{(2)}(a, b, c, \Lambda) \approx I_1(a, b, c, \Lambda), \end{aligned} \quad (65)$$

which is written up to certain $\mathcal{O}(1)$ numerical constants that are not relevant in studying the leading x -dependence of the structure functions. $I^{(1)}(M_1, M_3, \omega, \Lambda)$ is the integral which appears in the glueball case. Equation (65) implies that since we are working in the small Λ regime the larger contribution comes from the $\kappa = 4$ case, thus in what follows we will focus on this case. However, as we will see the contribution of the other integrals will become important in the $x \rightarrow 1$ limit. In addition, we can perform an approximation similar to the one we have used in [24]

$$\begin{aligned} I^{(4)}(a, b, c, \Lambda) &= \int_0^{\Lambda^{-1}} dz z^4 J_m(az) J_n(bz) J_l(cz) \\ &\approx \left(\frac{1}{\Lambda}\right)^3 \frac{1}{\sqrt{ab}} \left[(-1)^\alpha \delta(c - (a + b)) + (-1)^\beta \delta(c - (a - b)) \right], \end{aligned} \quad (66)$$

for some integer powers α and β that carry all the dependence on the indices of the Bessel functions¹³. The similarities between the different integrals come from the fact that, regardless of the integration limit, as functions of c their largest contribution comes from the region near $c = |a \pm b|$. In this context we have $\omega = M_1 \pm M_3$. This kind of behavior where bulk interactions in AdS act as some sort of energy conservation restriction has been noted before [25, 24], and in a sense it is an intuitive interpretation for the Dirac delta functions approximation (66).

¹³See Appendix C and also [41].

Considering this approximation for the IR vertex and, since both the UV vertex and the propagator $G(z, z')$ can be treated in the same way as for the glueball calculation, one can square the amplitude, perform the ω integration and carry out the angular integration in θ . The leading amplitude is given by $\omega = M_1 - M_3$. Then, the sum over M_3 indicates that the important contributions are given when the mass M_3 takes values near αM_1 , with $\alpha = |\vec{p}'|/|\vec{p}|$. All of these results indicate that the splitting occurs at small angles and that the ratio between the momentum carried by the on-shell resulting particle of mass M_3 and the momentum p of the incoming hadron is similar to that of the AdS masses¹⁴. Finally, we are left with the following M_2 sum

$$F_L^I = \frac{B^2}{\lambda N} \frac{M_1^6}{\Lambda^3} \sum_{M_2} \frac{M_2}{q^{14}} (M_2^2 + q^2)^2 x^6 (q^2(1-x) - xM_2^2)^3 x^6 \left(1 + \frac{M_2^2}{q^2}\right)^6, \quad (67)$$

where B is a numerical constant.

The difference between this sum and the glueball one is given by some constant factors Λ , but also M_3 and $\omega = M_1 - M_3$ which change the result as a function of x . Now, the leading contribution comes from the case where M_2 takes values of order q , which means that we can treat this sum as an integral with measure dM_2/Λ [23]. This integral gives the final result for the longitudinal structure function

$$F_L^{(I)}(x, q^2) = \frac{1}{\lambda N} \frac{B^2}{120} \left(\frac{M_1}{\Lambda}\right)^6 \frac{\Lambda^2}{q^2} x^3 (1-x)^4 (1 + 2x(2 + 5x)). \quad (68)$$

This is the most important result of this paper. However, since equation (68) behaves as $(1-x)^4$ when $x \rightarrow 1$ one has to keep in mind that there are other sub-leading z -integrals. These contributions render terms proportional to $x^3(1-x)^2(1+x(2+3x))$ and $x^3(1-x)^2$. This last term is exactly the one that appears in the glueball case. Notice that the x dependence is independent of the conformal dimension of the initial state. This is very different in comparison with the large N limit, as it has been noted for the glueball case [24]. Among the contributions coming from these terms, the one coming from the z^2 and z^3 integrals are the leading ones in this limit: when $x \rightarrow 1$ they behave as $(1-x)^2$. All other terms are sub-leading. The appearance of this asymptotic $(1-x)^2$ behavior is an important observation in terms of the comparison with phenomenology.

Notice that the upper index in equation (68) indicates that this is the leading contribution we have from the type I mode. Since we are using the optical theorem, we must add to this the other leading-order contribution that we have from the possibility that one of the intermediate states is associated with a type III mode. Details of the calculation are shown in Appendix B, being the final result of the same form as (68).

Finally, it is worth noticing that as expected in the leading structure function (68) (and also in the rest of the contributions) the q -dependence that one obtains is the same: the

¹⁴As in [24] we call $m^2 = R^{-2}\Delta(\Delta - 4)$ the Kaluza-Klein mass and M_i ($i = 1, 2, 3$) as the AdS masses.

amplitude fall off is Λ^2/q^2 . In the case of the glueballs this is predicted by OPE arguments on the quantum field theory side [23]. The gravitational interpretation of this is clear, when

$$q^2 > \Lambda^2 N^{2/(\tau_{\mathcal{Q}} - \tau_c)}, \quad (69)$$

the $1/N^2$ suppression for large (but finite) N of the one-loop level process and the $(\Lambda^2/q^2)^{\Delta_{in}-1}$ suppression factor of the tree-level amplitude becomes comparable, and for larger q the former calculation associated with two-particle final states DIS is the leading one¹⁵. In that case, one obtains a suppression factor Λ^2/q^2 . Thus, initial hadron splitting and particle creation are allowed. The scalar mode with lower Kaluza-Klein mass (i.e. with $\Delta_{min} = 2$) is the one propagating along the vertical line and interacting with the non-normalizable gauge field representing the holographic virtual photon. We expect the same interplay between these two terms in the $\mathcal{N} = 2$ SYM theory dual to the D3D7-brane model. An obvious difference is that instead of the factor $N^{2/(\tau_{\mathcal{Q}} - \tau_c)}$ in equation (69) we should have $N^{1/(\tau_{\mathcal{Q}} - \tau_c)}$ due to the fact that the fields in the hypermultiplet of the $\mathcal{N} = 2$ SYM theory transform in the fundamental representation of $SU(N)$.

4 Discussion and conclusions

In this work we have investigated the longitudinal structure function $F_L(x, q^2)$ for scalar mesons derived from the D3D7-brane model, at strong coupling and in the $1/N$ expansion. Equation (1) shows that the large N limit and the high energy limit ($\Lambda^2 \ll q^2$) do not commute. This is because $\Delta \geq 3$ for scalar mesons (see table 1), therefore in the $\Lambda^2 \ll q^2$ limit the first term is suppressed by (at least) an additional factor Λ^2/q^2 in comparison with the rest of terms. This implies that in this limit the second term in that equation becomes the leading contribution. Similarly to what happens with DIS of charged leptons off glueballs, we find that for scalar mesons two-hadron final states dominate DIS processes. In terms of the FCS this implies that certain one-loop Feynman-Witten diagrams in the supergravity calculation are the most relevant ones. Using some reasonable approximations explained in the preceding sections, we have obtained $F_L(x, q^2)$ in the high energy limit:

$$F_L = \frac{1}{N} \left(f_2^{(1)} - 2x f_1^{(1)} \right) \left(\frac{\Lambda^2}{q^2} \right).$$

Specifically we have obtained the expression (68), where we have calculated the explicit dependence on the Bjorken parameter when the FCS intermediate state corresponds to a type I mode, and a similar expression when the exchanged particle is a type III mode. These

¹⁵Note that $\tau_{\mathcal{Q}}$ is the minimum twist of a single-trace operators of charge \mathcal{Q} , and τ_c is the minimum twist of all electrically charged single-trace operators. In both cases the operator's anomalous dimensions are order 1.

two expressions behave as $(1-x)^4$ as x approaches 1. There are additional contributions from the sub-leading z -integrals which behave as $(1-x)^2$, however they are only relevant for x very close to 1, therefore their contribution to the moments of the structure functions is very small. Also, we have obtained the explicit dependence on the virtual photon momentum transfer q^2 .

We observe that the one-loop structure of the DIS amplitude leads to a non-vanishing F_1 structure function even for scalar hadrons, where this contribution is sub-leading in $1/N$. The leading term contribution to the DIS amplitude is given by F_2 , or in this case the longitudinal structure function $F_L = F_2 - 2xF_1$. We have obtained the full x -dependence for the Kaluza-Klein tower of scalar (and pseudoscalar) mesons. In all cases the key element comes from the analysis of the z -integral of the Bessel functions involved in the splitting process of the incoming hadron, followed by the sum over the intermediate masses M_2 and M_3 (see figure 1). A remarkable effect is that in equation (68) there is a factor $1/\lambda$ in addition to the $1/N$ factor. This is expected since the cubic interaction vertex involving three mesons has a coupling strength proportional to

$$g_{cubic} \propto \frac{1}{\sqrt{N}} \frac{\alpha'}{L}, \quad (70)$$

where $L = \Lambda R^2$ and since $R^2 = \sqrt{\lambda} \alpha'$ then

$$g_{cubic} \propto \frac{1}{\sqrt{N}} \frac{1}{\sqrt{\lambda}}. \quad (71)$$

There are several interesting aspects that we should emphasize. Firstly, the l dependence of the structure function appears only in the coefficients, but not in the powers of x or $(1-x)$. This is an important difference with respect to the structure functions in the $N \rightarrow \infty$ limit [5, 7], where $F_2 \propto x^{l+4}(1-x)^{l+1}$. This behavior has also been found for glueballs [24]. Secondly, for all mesons the structure function behaves as $F_L \sim (1-x)^2$ in the $x \approx 1$ region. This has already been pointed out in [7] for the pion, and the fact that it holds for the one-loop correction and extends to the rho meson constitutes an important test for the validity of our results. In the context of the valence structure functions it has been found a fall-off $(1-x)^{2\pm 0.1}$ [17].

The idea of this work is to show that the contribution of certain one-loop Feynman-Witten diagrams of FCS lead to a better agreement with lattice QCD simulations and phenomenological results for scalar mesons, in comparison with the tree-level calculations. Since the Bjorken parameter dependence of the results for F_L is independent of Δ_{in} it should hold for different scalar and pseudoscalar mesons. Thus, we have compared our results for the lightest pseudoscalar mesons from the D3D7-brane model with the pion, for which there are more available data. In fact the structure functions of the pion, and the associated parton distribution functions have been extensively studied allowing us to compare with data coming

from experiments and also from different phenomenological models [11, 12, 13, 14, 15, 16, 17], as well as from lattice QCD simulations [8, 9, 10].

The experiments carried out in order to analyze the internal structure of the pion are generally based on the Drell-Yan process within the parametric region $0.2 \leq x \leq 1$. This is approximately the range of values of $1/\sqrt{\lambda} \ll x < 1$ where the supergravity description is accurate, since the center-of-mass energy is not high enough in order to produce excited string states in the intermediate channels [23]. This is true at tree level, and in this work we have assumed that the absence of excited strings also holds at one-loop level. For smaller values of x supergravity is not a good description and one has to take into account the full string theoretical description in the holographic dual model, in that case string loop effects become important and, eventually, it could lead to black hole formation. Nevertheless, it is worth noticing that even when x is small some approximations can be done in order to describe the curved-space string theory scattering amplitude at high energy in terms of the flat-space ten-dimensional string theory scattering amplitude [23]. We have done this for scalar and polarized vector mesons in the $N \rightarrow \infty$ limit in [6], i.e. for single-hadron outgoing states. As we have pointed out in [7], in the multi-color limit the results in the $1/\sqrt{\lambda} \ll x < 1$ region, which one obtains from the holographic dual description of DIS of charged leptons off mesons in terms of supergravity, are well described in terms of the valence distribution functions. On the other hand, for smaller values of x the structure functions obtained from the inclusion of string theory effects seem to be associated with the contribution emerging from the soft gluons and the sea of quarks [6, 7].

Another important data to compare with are the first moments of the structure functions obtained from QCD lattice simulations. These moments are defined as

$$M_n[F_i] = \int_0^1 dx x^{n-1} F_i(x, q^2) , \quad (72)$$

for a generic structure function F_i . In [7] we have already analyzed our $N \rightarrow \infty$ results in terms of the moments of the pion and rho meson in comparison with the QCD lattice simulations results presented in [8]. In our holographic description of scalar mesons the lightest pseudoscalar one corresponds to the case where the initial and final states are described by the scalar fluctuation ϕ whose solution has the smallest Kaluza-Klein mass and couples to the $U(1)$ gauge field A_m given by a graviton. In the D3D7-brane model, the smallest $\Delta = l + 3$ corresponds to the case $l = 1$, where l indicates the irreducible representation of $SO(4) \sim SU(2) \times SU(2)$ of the associated scalar spherical harmonic.

The first three moments of $F_1(x, q^2)$ and $F_2(x, q^2)$ have been calculated from lattice QCD in [8] for the pion and the rho meson. We consider the moments of $F_2(x, q^2)$ for the pion and compare them with the moments of our $F_L(x, q^2)$ since in our case $F_1(x, q^2)$ is sub-leading. Thus, we integrate our result between $x = 0.1$ and $x = 1$, i.e. within the range of validity of the supergravity calculations (we refer this parametric region as the large- x region). However, since we are analyzing the first moments it is important to take into account the region for

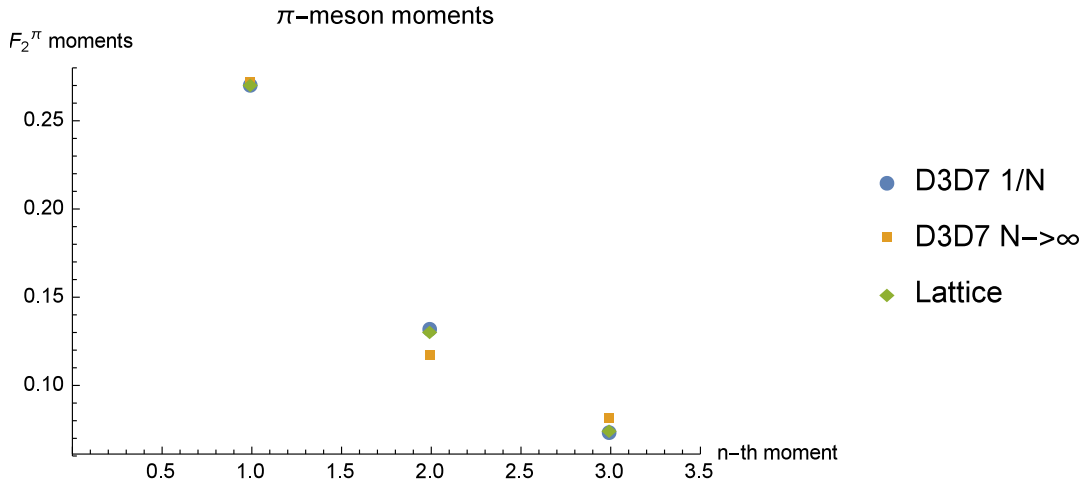


Figure 2: The first three moments of F_2 are shown for the pion. The free parameters of the D3D7-brane model are chosen in order to fit the results of [9, 10], obtained with lattice QCD simulations, and labeled by "Lattice QCD". Also, for comparison we have included the best fitting corresponding to the moments of the structure function in the large N limit, with errors up to 10.8% with respect to lattice QCD results. These are labeled by "D3D7 $N \rightarrow \infty$ ". "D3D7 $1/N$ " labels the best fitting corresponding to the moments of the structure function in the high energy limit, with errors up to 1.27% with respect to lattice QCD simulations [9, 10].

smaller values of x in order to be able to integrate the structure function for lower x values as well. We will assume that the small- x behavior is similar to the one we found in [6] and used in [7], i.e., $F_L^{small}(x, q^2) \propto x^{-1}$. The reason is given as follows. The main difference between our result for large- x in the one-loop calculation from the leading diagram of figure 1 and the previous one obtained in the planar limit is the fact that in the tree-level FCS calculation both the q - and x -dependence are determined by Δ_{in} of the target hadron, while at one-loop it is determined by Δ_{min} . Recall that Δ_{min} is given by the lowest conformal dimension available among the supergravity excitations. Nevertheless, at low- x the string theoretical calculation is independent of Δ_{in} . In this way, we may conjecture that in this aspect this will not be very different in comparison with the one-loop level situation. Thus, we consider this $1/x$ behavior and add it to the moment calculation by integrating it from $x = 0.0001$ and $x = 0.1$ as before [7]. We rewrite the rest of the structure function in two dimensionless constants: one in front of the small- x F_L part and the other one multiplying the large- x F_L part. Then, we carry out the best fitting for these two constants in comparison with the lattice QCD calculations of three lowest moments for the pion.

The results of that fitting are presented in figure 2 compared with the known results and the previous fitting performed with the $N \rightarrow \infty$ structure function F_2 . The first constants are approximately 0.0017 and 14.47. They are similar to the ones found in our previous work [7] in the large N limit, for which the constants associated with the small- x F_L and with

Model / Moment	$M_1(F_2)$	$M_2(F_2)$	$M_3(F_2)$
Lattice QCD	0.27	0.13	0.074
D3D7 (1/ N)	0.2699	0.1326	0.0731
Percentage error	0.04	-1.27	1.27
D3D7 ($N \rightarrow \infty$)	0.2708	0.1161	0.0803
Percentage error	-0.3	10.8	-8.5

Table 2: Comparison of our new results for the first moments of the structure function F_2 of the lightest pseudoscalar meson for a suitable choice of the normalization constants with respect to the average results of the lattice QCD simulations in [9, 10] and in comparison with the results presented in [7]. Uncertainties in the lattice computations are omitted.

the large- x F_L are 0.0143 and 28.89, respectively. Another interesting point is the ratio of the third and second moments of F_2 , which in large N limit gives $M_3[F_2]/M_2[F_2] = 0.69$ [7], while in the high energy limit gives $M_3[F_2]/M_2[F_2] = 0.55$. The last result is closer to the expected ratio near 0.5¹⁶.

Table 2 shows a comparison of our new results for the first three moments of the structure function F_2 of the lightest pseudoscalar meson with respect to the average results of the lattice QCD computations in [9, 10] and in comparison with the results presented in [7] at large N . Uncertainties in the lattice computations are omitted.

Also, the shape of the F_2 structure function as a function of the Bjorken parameter for fixed virtual photon momentum transfer is shown in figure 3. The darker line represents the present $1/N$ calculations, while the other curve corresponds to the previous ones reported in [7] in the large N limit. For low- x we consider our previous result from [6]. The difference between the two low- x curves is due to the slightly different constants needed for the best fitting in each situation. Also, notice that for the $1/N$ expansion for small- x F_L is smaller in comparison with the large N limit, while there is an opposite trend for the larger x region. In addition, as expected from phenomenological results the peak in F_L in the $1/N$ calculation moves toward smaller values of x .

Higher order moments can also be calculated from our results. We display these in figure 4 in comparison with [42]. The difference between the corresponding first moments of figure 4 and table 2 is due to the fact higher order moments are generally calculated from the valence structure functions and they do not include the small- x contributions.

The analysis of this work is restricted to the $1/N$ corrections to the holographic dual

¹⁶We thank Andreas Schafer for this comment.

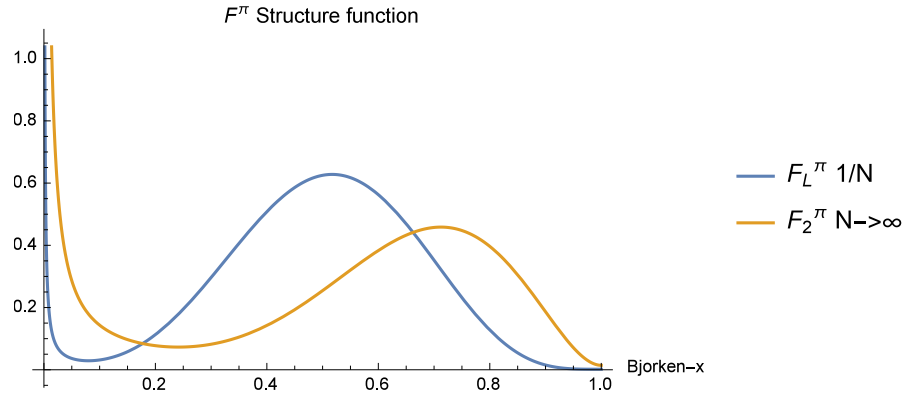


Figure 3: F_2 as a function of the Bjorken parameter x . We consider the values of the constants which give the moments indicated in table 2.

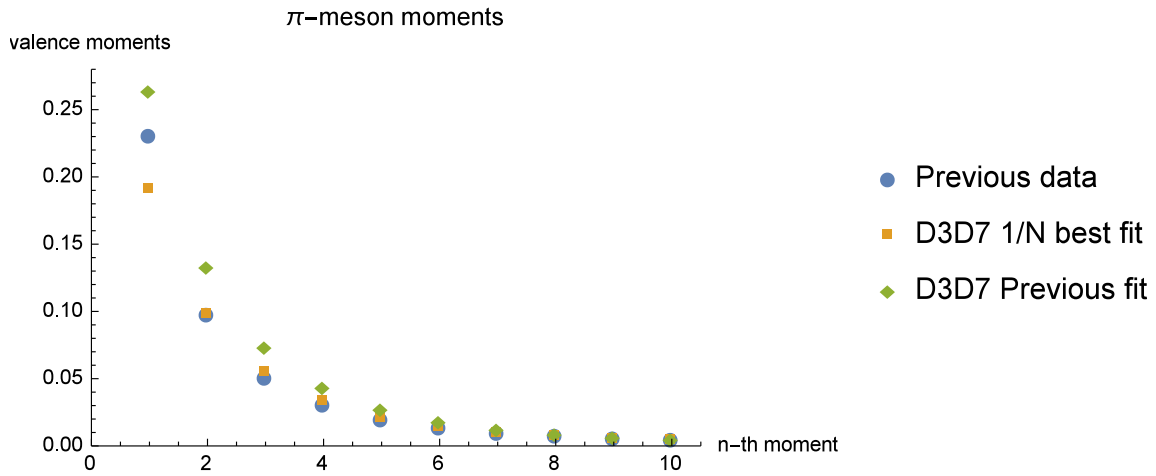


Figure 4: Higher moments of F_2 are shown for the pion. Previous data correspond to reference [42].

description of DIS of a charged lepton off scalar mesons. The Bjorken parameter dependence of the structure functions for higher orders in this expansion is difficult to calculate explicitly. However, we can comment on the q^2 -dependence of these terms. This dependence for the leading diagram is dictated by the UV interaction vertex, which has the same form as for the glueball case. In that situation the propagating mode is an s -scalar, also with the lowest conformal dimension [24]. Hence, it is reasonable to expect that at higher order in $1/N$ the splitting process will be more complicated, but still it will be restricted to the IR region. Note that for these ladder type higher-order diagrams there are in principle two possibilities: a type I $^-$ D7-brane field and the s -scalar bulk field. In any case the leading $1/q^2$ contribution should not change.

Let us very briefly comment on the $L = 0$ case which is very different for several reasons. Formally a null separation between the D7-brane and the stack of N D3-branes implies that conformal symmetry is restored, therefore the quarks become massless. This is because for k D7-branes the beta function for the 't Hooft coupling is proportional to k/N , which vanishes in the probe limit [1]. From the computational point of view, the crucial IR interaction vertex that couples the scalar mesons with any type of gauge modes is absent. In fact, except for the non-Abelian case (number of flavors larger than one) all three-point vertices vanish. This means that our leading diagram of figure 1 does not exist in this case. Thus, the results will be conceptually very different in this limit. For example, as in the previous paragraph one should go to higher orders in the $1/N$ expansion in order to find a diagram with a propagating mode carrying the lowest dimension. If the number of loops is increased one should also have higher powers of $1/\lambda$ multiplying the $1/N$ ones.

Possible extensions of this work to other gauge field theories can be done by considering the DpDp+4-brane models, which are duals to gauge theories in $p+1$ dimensions such as the ones discussed in [40].

Acknowledgments

We thank S. K. H. Auluck for correspondence on reference [41], and Ezequiel Koile, Gustavo Michalski and Carlos Núñez for comments and discussions. The work of D.J., N.K. and M.S. is supported by the CONICET. This work has been supported in part by the CONICET-PIP 0595/13 grant and UNLP grant 11/X648.

A Spherical harmonics on S^3

In this appendix we list some properties and formulas relevant for the type IIB supergravity Feynman diagram calculation at one-loop level that we use in order to obtain the structure functions of scalar mesons in the $1/N$ expansion. Several of the basic results involving scalar and vector spherical harmonics have been derived in [43] and [44].

A.1 Basic properties of spherical harmonics

Spherical harmonics belong to representations of the isometry group of the three-sphere, i.e. $SO(4) \approx SU(2) \times SU(2)$. The scalar spherical harmonics transform in the $(\frac{l}{2}, \frac{l}{2})$ representation, where l is a non-negative integer, while $-\frac{l}{2} \leq m, n \leq \frac{l}{2}$. They satisfy an orthogonality condition

$$\int_{S^3} Y_l^{m,n} Y_{l'}^{m',n'} = \delta_{ll'} \delta_{mn} \delta_{m'n'}, \quad (73)$$

and their complex conjugate are calculated from

$$(Y_l^{m,n})^* = (-1)^{m+n} Y_l^{-m,-n}. \quad (74)$$

Spherical harmonics are eigenfunctions of the Laplace operator on the sphere

$$\nabla^2 Y_l^{m,n} = -l(l+2) Y_l^{m,n}. \quad (75)$$

Under parity transformation their eigenvalues are $(-1)^l$.

A vector field on S^3 can be spanned by a combination of gradients of the scalar spherical harmonics $\nabla_i Y$ plus a set of vector spherical harmonics Y_i^\pm , which transform in the $(\frac{l\pm 1}{2}, \frac{l\pm 1}{2})$ representation of the $SO(4) \approx SU(2) \times SU(2)$ group, with $l \geq 1$. In order to make the notation simpler, the indices m and n can be omitted. Whenever it is necessary to write them explicitly, we use the following notation $\vec{Y}_{l,\epsilon}^{m,n}$, where $\epsilon = \pm 1$ indicate the representation. They satisfy the eigenvalue equations

$$\nabla_i \nabla^i Y_j^{l,\pm} - R_j^k Y_k^{l,\pm} = -(l+1)^2 Y_j^{l,\pm}, \quad (76)$$

$$\epsilon_{ijk} \nabla_j Y_k^{l,\pm} = \pm(l+1) Y_i^{l,\pm}, \quad (77)$$

$$\nabla^i Y_i^{l,\pm} = 0, \quad (78)$$

where $R_{ij} = 2\delta_{ij}$ is the Ricci tensor of an S^3 of unit radius. Also, they satisfy the following relation

$$\vec{Y}_{l,\epsilon}^{*,m,n} = (-1)^{m+n+1} \vec{Y}_{l,\epsilon}^{-m,-n}. \quad (79)$$

The vector spherical harmonics satisfy orthogonality relations,

$$\begin{aligned} \int_{S^3} \vec{Y}_{l,\epsilon}^{m,n} \cdot \vec{Y}_{l',\epsilon'}^{m',n'} &= \delta_{l,l'} \delta_{m,m'} \delta_{n,n'} \delta_{\epsilon,\epsilon'}, \\ \int_{S^3} \vec{Y}_{l,\epsilon}^{m,m'} \cdot \vec{\nabla} Y_{l'}^{n,n'} &= 0. \end{aligned} \quad (80)$$

The $\vec{Y}_{l,\epsilon}^{m,n}$ harmonics does not mix with other vector spherical harmonics since they belong to different representations of $SO(4)$.

A.2 Integrals of spherical harmonics

The interaction vertices we consider have coefficients involving integrals over three spherical harmonics. These integrals lead to selection rules for the outgoing modes and introduce a dependence in l . The relevant integrals are,

$$\int_{S^3} Y_l^{m,n} \vec{Y}_{l',\epsilon}^{m',n'} \cdot \vec{Y}_{l'',\epsilon''}^{m'',n''} = \begin{pmatrix} \frac{l'+\epsilon}{2} & \frac{l''+\epsilon''}{2} & \frac{l}{2} \\ m' & m'' & m \end{pmatrix} \begin{pmatrix} \frac{l'-\epsilon}{2} & \frac{l''-\epsilon''}{2} & \frac{l}{2} \\ n' & n'' & n \end{pmatrix} R_{1,\epsilon,\epsilon'}(l', l, l'') \quad (81)$$

$$\int_{S^3} Y_l^{m,n} \vec{Y}_{l',\epsilon}^{m',n'} \cdot \nabla Y_{l''}^{m'',n''} = \begin{pmatrix} \frac{l''}{2} & \frac{l'+\epsilon'}{2} & \frac{l}{2} \\ m'' & m' & m \end{pmatrix} \begin{pmatrix} \frac{l''}{2} & \frac{l'-\epsilon'}{2} & \frac{l}{2} \\ n'' & n' & n \end{pmatrix} R_2(l', l, l''), \quad (82)$$

where the matrices are the $3j$ -symbols, while the functions R_1 and R_2 are defined as

$$\begin{aligned} R_{1,\epsilon,\epsilon'}(x, y, z) &= \frac{(-1)^{\sigma+(\epsilon+\epsilon')/2}}{\pi} \left(\frac{(y+1)}{32(x+1)(z+1)} \right)^{1/2} ((\epsilon(x+1) + \epsilon'(z+1) + y + 2) \\ &\quad (\epsilon(x+1) + \epsilon'(z+1) + y)(\epsilon(x+1) + \epsilon'(z+1) - y) \\ &\quad (\epsilon(x+1) + \epsilon'(z+1) - y - 2))^{1/2}, \end{aligned} \quad (83)$$

$$R_2(x, y, z) = \frac{(-1)^{\sigma'}}{\pi} \left[\frac{(x+1)(z+1)(\sigma'-x)(\sigma'-y)(\sigma'-z)(\sigma'+1)}{(y+1)} \right]^{\frac{1}{2}}. \quad (84)$$

The right-hand sides of these equations are defined to be non-vanishing only if the inequality $|x-z| \leq y \leq x+z$ is fulfilled, and if $\sigma = \frac{x+y+z}{2}$ in R_1 and $\sigma' = \frac{x+y+z+1}{2}$ in R_2 are integers.

The leading diagram in the $1/N$ expansion has an incoming scalar meson, a vector type I ($\epsilon = -1$) mode with $l = 1$, and a third field which could be a type I or type III mode. The intermediate meson with $l = 1$ only admits $m' = 0$ and the n' index can take three possible values $(\pm 1, 0)$. Firstly, we consider the case with a type I ($\epsilon = -1$) scalar as the third field in the vertex. The angular integral is

$$\int_{S^3} Y_l^{m,n} \vec{Y}_{1,-1}^{m',n'} \cdot \vec{Y}_{l'',-1}^{m'',n''} = \begin{pmatrix} \frac{l''-1}{2} & 0 & \frac{l}{2} \\ m'' & 0 & m \end{pmatrix} \begin{pmatrix} \frac{l''+1}{2} & 1 & \frac{l}{2} \\ n'' & n' & n \end{pmatrix} R_{3,-1,-1}(l'', l, 1). \quad (85)$$

The first j -symbol imposes a selection rule on l''

$$\begin{pmatrix} \frac{l'-1}{2} & 0 & \frac{l}{2} \\ m & 0 & -m \end{pmatrix} = \begin{cases} (-1)^{-m} \frac{i^{-l}}{\sqrt{l+1}} & \text{if } l'' = l + 1 \\ 0 & \text{if } l'' \neq l + 1. \end{cases} \quad (86)$$

From the conservation conditions $m + m' = 0$ and $n + n' + n'' = 0$, we can simplify the integral and calculate the sum of the square terms by using the optical theorem

$$\sum_{n'=-1}^1 \left(\begin{pmatrix} \frac{l}{2} & 0 & \frac{l}{2} \\ -m & 0 & m \end{pmatrix} \begin{pmatrix} \frac{l+2}{2} & 1 & \frac{l}{2} \\ -n-n' & n' & n \end{pmatrix} R_{3,-1,-1}(l, l+1, 1) \right)^2 = \frac{1}{2\pi^2}. \quad (87)$$

The result is independent of the conformal dimension related to the incoming field ($\Delta \sim l$). If the third mode is a type I scalar with $\epsilon = 1$ the j -symbols change and the selection rule is $l'' = l - 1$, but the result is the same. However, for a type III scalar we obtain a selection rule $l = l''$ and the result depends on the conformal dimension of the incoming field

$$\sum_{n'=-1}^1 \left(\begin{pmatrix} \frac{l}{2} & 0 & \frac{l}{2} \\ m & 0 & -m \end{pmatrix} \begin{pmatrix} \frac{l}{2} & 1 & \frac{l}{2} \\ -n-n' & n' & n \end{pmatrix} R_2(l, l, 1) \right)^2 = \frac{l(l+2)}{2\pi^2}. \quad (88)$$

B Contribution of the type III mode

Let us consider an outgoing type III mode. In eight dimensions the solution is defined by two functions $\phi_{III}(\rho)$ and $\tilde{\phi}_{III}(\rho)$, and the scalar spherical harmonics $Y^{(l)}(\Omega)$ of S^3 . It takes the form [1]

$$B_\mu = 0 \quad , \quad B_\rho = e^{ik \cdot x} \phi_{III}(\rho) Y^{(l)}(\Omega) \quad , \quad B_i = e^{ik \cdot x} \tilde{\phi}_{III}(\rho) \nabla_i Y^{(l)}(\Omega) \quad , \quad (89)$$

where the associated conformal dimension is $\Delta = l + 3$ and the relation between the radial functions is

$$l(l+2) \tilde{\phi}_{III} = \frac{1}{\rho} \partial_\rho (\rho^3 \phi_{III}) \quad . \quad (90)$$

The equation of motion is given by

$$\partial_\rho \left(\frac{1}{\rho} \partial_\rho (\rho^3 \phi_{III}(\rho)) \right) - l(l+2) \phi_{III}(\rho) - \frac{M^2 R^2}{\rho^2} \phi_{III}(\rho) = 0 \quad , \quad (91)$$

where we have taken L very small. Since L appears only at quadratic order in equation (91), we can use the $L = 0$ solutions for the on-shell evaluation instead of the Hypergeometric ones corresponding to non-zero values of L . Then, the normalizable solutions are given in terms of Bessel functions is $\phi_{III} = c_{III} J_{\Delta-2}(MR^2/\rho)$ where $c_{III} = R^2 \sqrt{l(l+2)} \Lambda/M$. Note

that these modes have a different normalization constant in comparison with the mode I. Plugging this expression in the on-shell interaction action given in equation (52), the first two terms of the effective action vanish. Thus

$$\int d\Omega_3 Y^{l''} \nabla^i Y^{1j} \left(\nabla_i \nabla_j Y^{*l} - \nabla_j \nabla_i Y^{*l} \right) = 0. \quad (92)$$

Therefore, we obtain the following expression for the on-shell evaluation of the interaction action

$$S_{int} = -\frac{\mu_7}{N^{3/2}} (2\pi\alpha')^3 2L \int d\rho d\Omega_3 \sqrt{-g} \frac{\phi(\rho)}{\rho^2} \nabla^\rho(\phi_I(\rho)) \left(\partial_\rho \tilde{\phi}_{III}(\rho) - \phi_{III}(\rho) \right) Y^{in} Y^{Ii} \nabla_i Y^{III}, \quad (93)$$

where we have omitted the momentum conservation factor as before. This can be simplified by using the relation between $\tilde{\phi}_{III}$ and ϕ_{III} of equation (90) and the equation of motion, since they imply

$$\nabla_\rho(\tilde{\phi}_{III}(\rho)) = \frac{\partial_\rho \left(\frac{1}{\rho} \partial_\rho (\rho^3 \phi_{III}(\rho)) \right)}{l(l+2)} = \phi_{III} \left(1 + \frac{M_3^2 R^4}{l(l+2)\rho^2} \right). \quad (94)$$

The resulting action in terms of $z = R^2/\rho$ for the outgoing type III mode is

$$S_{int} = -\frac{\mu_7}{N^{3/2}} (2\pi\alpha')^3 2L \sqrt{\frac{M_3 M_1 \omega}{l(l+2)}} M_3 \int dz z^2 \partial_z (z^2 J_0(\omega z)) J_{\Delta_{in}-2}(M_1 z) J_{\Delta_3-2}(M_3 z) I_3, \quad (95)$$

where $I_3 = \int d\Omega_3 Y^{(in)} \vec{Y}^I \cdot \nabla Y^{III}$ is the angular integral on the sphere which it is performed in Appendix A. As we can see, the z -integrals have powers of order 3 and 4 as for the type I case. Now, one can insert this on-shell S_{int} in the holographic expression for the electromagnetic current one-point function with the corresponding two-particle final state. This leads to a non-vanishing contribution to the longitudinal structure function of the same form as in the type I case. The M_3^2 factor is canceled with the normalization constant of the modes III. In addition, the factor $\sqrt{l(l+2)}$ in the denominator, which introduces a Δ dependence, is canceled by the angular integral on S^3 .

C Integrals of products of Bessel functions

In this appendix we discuss the approximations of the z -integrals of three Bessel functions at the IR interaction vertex that we use to obtain the structure functions in Section 3.5.

In the case of glueballs [24], the IR interaction vertex describes a process where an incoming hadron, whose holographic dual representation is given by a normalizable Kaluza-Klein mode of the dilaton, splits into two other hadrons. Similarly, in the present case for scalar

mesons, in the leading contribution one of the two resulting fields has the minimal conformal dimension Δ_{min} . This is $\Delta_{min} = 2$, and it is the same both for glueballs [24] and for scalar mesons. Considering the change of variable $z = R^2/r$, the on-shell interaction action involves a z -integral of the form

$$I^{(1)} = \int_0^{z_{max}} dz z J_{\Delta_{in}-2}(M_1 z) J_{\Delta'-2}(M_3 z) J_0(\omega z), \quad z_{max} = \Lambda^{-1}. \quad (96)$$

This kind of integrals are not explicitly known for arbitrary integration limits. The known analytic results are obtained when the upper limit is $z \rightarrow \infty$, and they can be written in terms of Hypergeometric functions and Appell series [45]. However, an interesting numerical analysis has been developed by Auluck. In [41], it has been proposed that as a function of one of the AdS masses, ω , and in the limit of large z_{max} the integral of equation (96) behaves approximately as a sum of Dirac delta functions, up to some normalization constant. It is easy to see how these functions arise. By using the asymptotic expression¹⁷ (57) it allows one to rewrite a general product of three Bessel functions $J_m(az) J_n(bz) J_l(cz)$ as

$$\begin{aligned} & \left(\frac{2}{\pi z}\right)^{3/2} \frac{1}{\sqrt{abc}} \cos\left(az - m\frac{\pi}{2} - \frac{\pi}{4}\right) \cos\left(bz - n\frac{\pi}{2} - \frac{\pi}{4}\right) \cos\left(cz - l\frac{\pi}{2} - \frac{\pi}{4}\right) \\ &= \left(\frac{2}{\pi z}\right)^{3/2} \frac{1}{\sqrt{abc}} \sum_{\alpha=\pm 1, \beta=\pm 1} \cos\left[(c - \alpha a - \beta b)z + (-m + \alpha n + \beta l)\frac{\pi}{2} + (-1 + \alpha + \beta)\frac{\pi}{4}\right]. \end{aligned} \quad (97)$$

Now, the integration of each term multiplied by z leads to the appearance of the square of the corresponding frequency, plus some signs and Fresnel sine and cosine functions. These frequencies are given by $|c \pm a \pm b|$, and each term describes the correct behavior near the region where one of these factors vanishes. In our case it means that the integral has two divergencies, namely: at $\omega = (M_1 \pm M_3)$. Another way to see this is to proceed as in [46] by using the analytic continuation of the series expansion of the Bessel functions

$$J_m(az) \approx \frac{1}{\sqrt{2\pi az}} \left[e^{i(az - m\frac{\pi}{2} - \frac{\pi}{4})} \sum_{j=0}^{\infty} \frac{i^j(m, j)}{(2az)^j} + e^{-i(az - m\frac{\pi}{2} - \frac{\pi}{4})} \sum_{j=0}^{\infty} \frac{i^{-j}(m, j)}{(2az)^j} \right], \quad (98)$$

where

$$(m, j) \equiv \frac{\Gamma\left(\frac{1}{2} + m + j\right)}{n! \Gamma\left(\frac{1}{2} + m - j\right)}.$$

By combining this expression for each Bessel function, multiplying by z and integrating term by term, one obtains the same poles as before plus finite terms. Thus, scaling arguments for the behavior of the integral under the change $(a, b, c) \rightarrow (ka, kb, kc)$ for some constant k ,

¹⁷Since the hadron splitting occurs in the IR region this approximation makes sense because the main contribution to the z -integral comes from values of z far away from zero.

together with a numerical analysis similar to the one of reference [41] around each singularity, lead to an approximation in terms of two Dirac delta functions. It takes the form

$$I^{(1)} \approx \frac{1}{\sqrt{M_1 M_3}} [(-1)^{\gamma_-} \delta(\omega - (M_1 - M_3)) + (-1)^{\gamma_+} \delta(\omega - (M_1 + M_3))] , \quad (99)$$

where γ_{\pm} can be 0 or 1 according to the phases determined by the (m, n, l) indices in the asymptotic approximation (97). They are not important for the present calculation, since we only need the square of the first term. There is a simple physical interpretation for this Dirac delta function behavior: it is associated with some sort of mass-conservation condition in the IR process [25, 24].

In the present case, the situation seems to be more complicated since we have a linear combination of different integrals of the form

$$I^{(\kappa)} = \int_0^{z_{max}} dz z^{\kappa} J_{\Delta_{in}-2}(M_1 z) J_{\Delta'-2}(M_3 z) J_0(\omega z) , \quad (100)$$

with $\kappa = 2, 3, 4$. Naively, it seems that we might have a problem since for $z_{max} \rightarrow \infty$ the integrand grows (and oscillates) with z for $\kappa \geq 3/2$. However, we are not integrating up to $z = \infty$ and the fact that there is an upper limit given by the cut-off is important. In addition, there would be no problem even if there was no cut-off: one has to keep in mind that the Bessel function solutions are only an approximation. The background is not exactly $AdS_5 \times S^3$ and the exact form of the solutions is given in [1] in terms of Hypergeometric functions. The product of three of them times z^{κ} falls off for any κ for large z for all the values of κ we are dealing with. We do not see this explicitly because this behavior occurs at distances larger than $z \sim R^2/L$, where the approximation breaks down. On the other hand, a similar analysis singles out the same singularities on the ω -plane. Now, all of this encourages us to consider an analogous approximation to what was used in the glueball calculation for $\kappa = 1$, and we only need to study the behavior near $\omega = M_1 \pm M_3$.

We find that these integrals behave very similarly when they are divided by an appropriate power of the upper limit of integration. The observed numerical behavior is depicted by some examples where each integral is studied as a function of Λ^{-1} for different values of ω (figures 5, 6 and 7). From these figures we can see that $\Lambda I^{(2)}$, $\Lambda^2 I^{(3)}$ and $\Lambda^3 I^{(4)}$ behave in the same way, up to some $\mathcal{O}(1)$ numerical constants, and very similarly to $I^{(1)}$.

In fact, one can see directly this from (97) by performing first an indefinite integral in z for the four different cases, obtaining

$$\begin{aligned} \int dz z^{-1/2} \cos(Pz + b) &= \left(\frac{2\pi}{P}\right)^{1/2} \left[\cos(b)C(\sqrt{2\pi^{-1}Pz}) - \sin(b)S(\sqrt{2\pi^{-1}Pz}) \right] \\ \int dz z^{1/2} \cos(Pz + b) &= \left(\frac{2\pi}{4P^3}\right)^{1/2} \left[-\cos(b)S(\sqrt{2\pi^{-1}Pz}) - \sin(b)C(\sqrt{2\pi^{-1}Pz}) \right. \\ &\quad \left. + 2\sqrt{Pz} \sin(Pz + b) \right] \end{aligned}$$

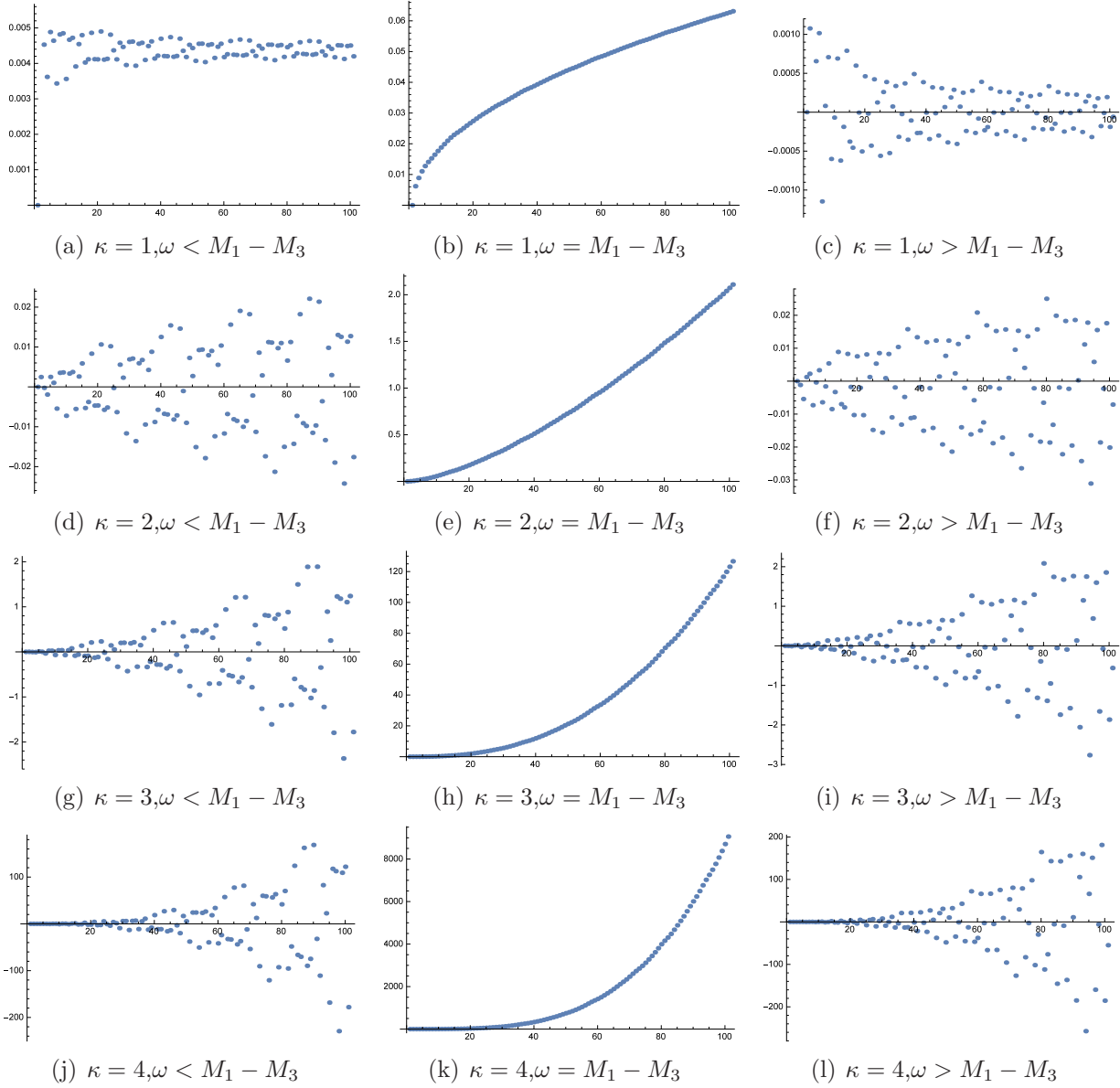


Figure 5: Examples of the integrals $I^{(\kappa)}(\Lambda)$ numerically evaluated for $\kappa = 1, \dots, 4$ and shown as a function of the upper integration limit Λ^{-1} . The parameters used are $M_1 = 15$, $M_3 = 6$ and $\omega = 7, 9, 11$ respectively.

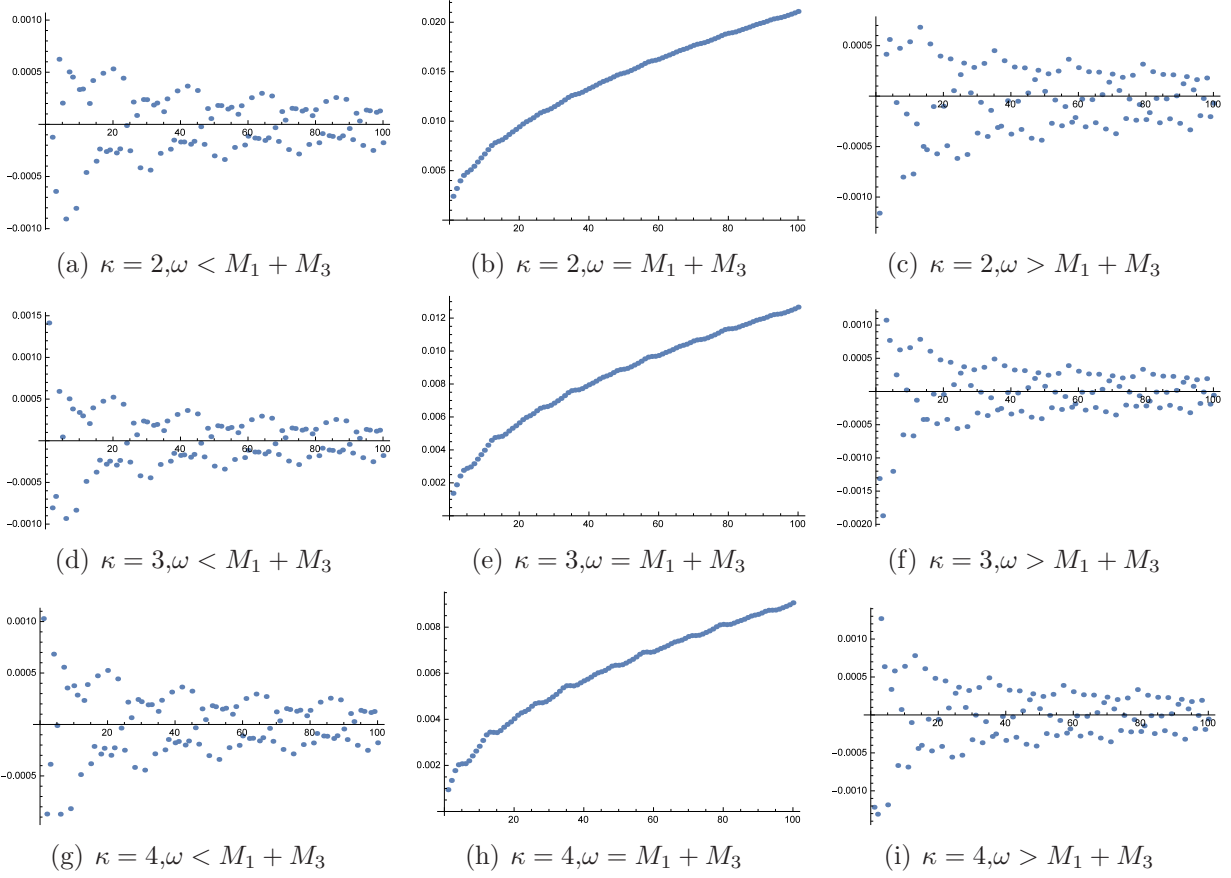


Figure 6: The rescaled integrals $\Lambda^{\kappa-1} I^{(\kappa)}(\Lambda)$ are numerically evaluated for $\kappa = 2, \dots, 4$ and shown as a function of the upper integration limit Λ^{-1} . The parameters used are $M_1 = 15$, $M_3 = 6$ and $\omega = 7, 9, 11$ respectively. The different behaviors depicted in the previous figure disappear (up to an order 1 constant) and the results for each ω are similar for all integrals. One can see that in all cases the integral decreases (or gives a small constant) for all values of $\omega \neq \omega_c = M_1 - M_3$.

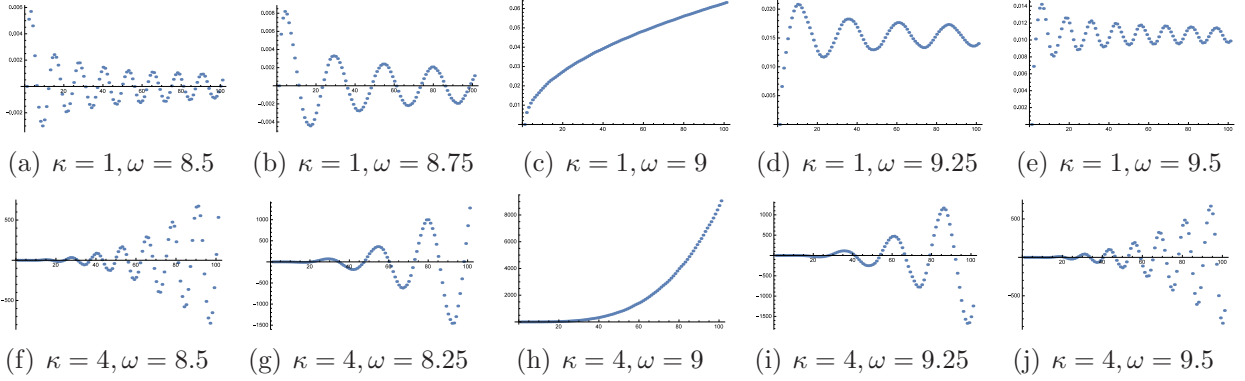


Figure 7: The behavior of integrals $I^{(\kappa)}(\Lambda)$ with $\kappa = 1$ and $\kappa = 4$ near the peak is shown using diagrams similar to the ones in the previous figures but with $\omega = 8.5, 8.75, 9, 9.25$ and 9.5 in both cases.

$$\int dz z^{3/2} \cos(Pz + b) = \frac{1}{4} \left(\frac{2\pi}{P^5} \right)^{1/2} \left[-3 \cos(b) C(\sqrt{2\pi^{-1}Pz}) + 3 \sin(b) S(\sqrt{2\pi^{-1}Pz}) \right. \\ \left. + 2\sqrt{Pz} (3 \cos(Pz + b) + 2Pz \sin(Pz + b)) \right]$$

$$\int dz z^{5/2} \cos(Pz + b) = \frac{1}{8} \left(\frac{2\pi}{P^7} \right)^{1/2} \left[15 \cos(b) S(\sqrt{2\pi^{-1}Pz}) + 15 \sin(b) C(\sqrt{2\pi^{-1}Pz}) \right. \\ \left. + 2\sqrt{Pz} (10Pz \cos(Pz + b) + (4P^2 z^2 - 15) \sin(Pz + b)) \right]$$

where P stands for the deviation from $\omega = M_1 \pm M_3$ and b represents some phase, while $S(x)$ and $C(x)$ are the Fresnel sine and cosine functions, respectively. Now, evaluating these results between $z = 0$ and $z = \Lambda^{-1}$ and expanding around the peak, i.e., around $P = 0$ one finds that, at least in this parametric region, the different integrals are related as stated in our approximation.

The reason for this behavior is that as the integrands of the $I^{(n)}$ integrals grow with z up to z_{max} , the most important contribution comes from the region $z \sim z_{max} = \Lambda^{-1}$. This was already noticed in the study of the normalization of the wave function of an incoming glueball in [23]. Scaling arguments under the change $(a, b, c) \rightarrow (ka, kb, kc)$ also agree with this analysis. Therefore, the approximation we use is given by equations (65) and (66).

References

- [1] M. Kruczenski, D. Mateos, R. C. Myers, D. J. Winters, “Meson spectroscopy in AdS / CFT with flavor,” *JHEP* **0307** (2003) 049. [arXiv:hep-th/0304032 [hep-th]].
- [2] M. Kruczenski, D. Mateos, R. C. Myers and D. J. Winters, “Towards a holographic dual of large $N(c)$ QCD,” *JHEP* **0405** (2004) 041 [hep-th/0311270].
- [3] T. Sakai, S. Sugimoto, “Low energy hadron physics in holographic QCD,” *Prog. Theor. Phys.* **113** (2005) 843-882. [arXiv:hep-th/0412141 [hep-th]].
- [4] E. Koile, S. Macaluso and M. Schvellinger, “Deep Inelastic Scattering from Holographic Spin-One Hadrons,” *JHEP* **1202**, 103 (2012) [arXiv:1112.1459 [hep-th]].
- [5] E. Koile, S. Macaluso and M. Schvellinger, “Deep inelastic scattering structure functions of holographic spin-1 hadrons with $N_f \geq 1$,” *JHEP* **1401**, 166 (2014) [arXiv:1311.2601 [hep-th]].
- [6] E. Koile, N. Kovensky and M. Schvellinger, “Hadron structure functions at small x from string theory,” *JHEP* **1505** (2015) 001 [arXiv:1412.6509 [hep-th]].
- [7] E. Koile, N. Kovensky and M. Schvellinger, “Deep inelastic scattering cross sections from the gauge/string duality,” *JHEP* **1512** (2015) 009 [arXiv:1507.07942 [hep-th]].
- [8] C. Best, M. Gockeler, R. Horsley, E. M. Ilgenfritz, H. Perlt, P. E. L. Rakow, A. Schafer and G. Schierholz *et al.*, “Pion and rho structure functions from lattice QCD,” *Phys. Rev. D* **56**, 2743 (1997) [hep-lat/9703014].
- [9] D. Brommel *et al.* [QCDSF-UKQCD Collaboration], “Quark distributions in the pion,” *PoS LAT* **2007** (2007) 140.
- [10] L. Chang, C. Mezrag, H. Moutarde, C. D. Roberts, J. Rodríguez-Quintero and P. C. Tandy, “Basic features of the pion valence-quark distribution function,” *Phys. Lett. B* **737** (2014) 23 doi:10.1016/j.physletb.2014.08.009 [arXiv:1406.5450 [nucl-th]].
- [11] K. Wijesooriya, P. E. Reimer and R. J. Holt, “The pion parton distribution function in the valence region,” *Phys. Rev. C* **72**, 065203 (2005) [nucl-ex/0509012].
- [12] R. J. Holt and C. D. Roberts, “Distribution Functions of the Nucleon and Pion in the Valence Region,” *Rev. Mod. Phys.* **82**, 2991 (2010) [arXiv:1002.4666 [nucl-th]].
- [13] P. Reimer, R. Holt and K. Wijesooriya, “The Partonic Structure of the Pion at Large- x ,” *AIP Conference Proceedings* 1369, 153 (2011); doi: 10.1063/1.3631531

- [14] L. Chang and A. W. Thomas, “Pion Valence-quark Parton Distribution Function,” arXiv:1410.8250 [nucl-th].
- [15] W. Detmold, W. Melnitchouk and A. W. Thomas, “Parton distribution functions in the pion from lattice QCD,” Phys. Rev. D **68**, 034025 (2003) [hep-lat/0303015].
- [16] M. Aicher, A. Schafer and W. Vogelsang, “Threshold-Resummed Cross Section for the Drell-Yan Process in Pion-Nucleon Collisions at COMPASS,” Phys. Rev. D **83**, 114023 (2011) [arXiv:1104.3512 [hep-ph]].
- [17] M. Aicher, A. Schafer and W. Vogelsang, “Soft-gluon resummation and the valence parton distribution function of the pion,” Phys. Rev. Lett. **105**, 252003 (2010) [arXiv:1009.2481 [hep-ph]].
- [18] H. B. Meyer and M. J. Teper, “Glueball Regge trajectories and the pomeron: A Lattice study,” Phys. Lett. B **605** (2005) 344 [hep-ph/0409183].
- [19] H. Meyer and M. Teper, “Confinement and the effective string theory in $SU(N \rightarrow \infty)$: A Lattice study,” JHEP **0412** (2004) 031 [hep-lat/0411039].
- [20] H. B. Meyer, “Glueball regge trajectories,” hep-lat/0508002.
- [21] G. S. Bali, F. Bursa, L. Castagnini, S. Collins, L. Del Debbio, B. Lucini and M. Panero, “Mesons in large- N QCD,” JHEP **1306** (2013) 071 [arXiv:1304.4437 [hep-lat]].
- [22] G. S. Bali, L. Castagnini, B. Lucini and M. Panero, “Large- N mesons,” PoS LATTICE **2013** (2014) 100 [arXiv:1311.7559 [hep-lat]].
- [23] J. Polchinski and M. J. Strassler, “Deep inelastic scattering and gauge / string duality,” JHEP **0305**, 012 (2003) [hep-th/0209211].
- [24] D. Jorjin, N. Kovensky and M. Schvellinger, “Towards $1/N$ Corrections to Deep Inelastic Scattering from the Gauge/Gravity Duality,” JHEP **1604** (2016) 113 [arXiv:1601.01627 [hep-th]].
- [25] J. H. Gao and Z. G. Mou, “Structure functions in deep inelastic scattering from gauge/string duality beyond single-hadron final states,” Phys. Rev. D **90**, no. 7, 075018 (2014) [arXiv:1406.7576 [hep-ph]].
- [26] J. Erlich, E. Katz, D. T. Son and M. A. Stephanov, “QCD and a holographic model of hadrons,” Phys. Rev. Lett. **95** (2005) 261602 [hep-ph/0501128].
- [27] L. Da Rold and A. Pomarol, “Chiral symmetry breaking from five dimensional spaces,” Nucl. Phys. B **721** (2005) 79 [hep-ph/0501218].

- [28] T. Hambye, B. Hassanain, J. March-Russell and M. Schvellinger, “On the Delta $I = 1/2$ rule in holographic QCD,” *Phys. Rev. D* **74** (2006) 026003 [hep-ph/0512089].
- [29] T. Hambye, B. Hassanain, J. March-Russell and M. Schvellinger, “Four-point functions and Kaon decays in a minimal AdS/QCD model,” *Phys. Rev. D* **76** (2007) 125017 [hep-ph/0612010].
- [30] S. Caron-Huot, P. Kovtun, G. D. Moore, A. Starinets and L. G. Yaffe, “Photon and dilepton production in supersymmetric Yang-Mills plasma,” *JHEP* **0612** (2006) 015 [arXiv:hep-th/0607237].
- [31] B. Hassanain and M. Schvellinger, “Diagnostics of plasma photoemission at strong coupling,” *Phys. Rev. D* **85** (2012) 086007 [arXiv:1110.0526 [hep-th]].
- [32] B. Hassanain and M. Schvellinger, “Plasma conductivity at finite coupling,” *JHEP* **1201** (2012) 114 [arXiv:1108.6306 [hep-th]].
- [33] B. Hassanain, M. Schvellinger, “Towards ’t Hooft parameter corrections to charge transport in strongly-coupled plasma,” *JHEP* **1010** (2010) 068 [arXiv:1006.5480 [hep-th]].
- [34] B. Hassanain and M. Schvellinger, “Plasma photoemission from string theory,” *JHEP* **1212** (2012) 095 [arXiv:1209.0427 [hep-th]].
- [35] G. Aarts, C. Allton, J. Foley, S. Hands and S. Kim, “Spectral functions at small energies and the electrical conductivity in hot, quenched lattice QCD,” *Phys. Rev. Lett.* **99** (2007) 022002 [hep-lat/0703008 [HEP-LAT]].
- [36] Y. Hatta, E. Iancu and A. H. Mueller, “Deep inelastic scattering at strong coupling from gauge/string duality: The Saturation line,” *JHEP* **0801** (2008) 026 [arXiv:0710.2148 [hep-th]].
- [37] Y. Hatta, E. Iancu and A. H. Mueller, “Deep inelastic scattering off a $N=4$ SYM plasma at strong coupling,” *JHEP* **0801** (2008) 063 [arXiv:0710.5297 [hep-th]].
- [38] B. Hassanain and M. Schvellinger, “Holographic current correlators at finite coupling and scattering off a supersymmetric plasma,” *JHEP* **1004** (2010) 012 [arXiv:0912.4704 [hep-th]].
- [39] H. J. Kim, L. J. Romans and P. van Nieuwenhuizen, “The Mass Spectrum of Chiral $N=2$ $D=10$ Supergravity on S^{*5} ,” *Phys. Rev. D* **32** (1985) 389. doi:10.1103/PhysRevD.32.389
- [40] R. C. Myers and R. M. Thomson, “Holographic mesons in various dimensions,” *JHEP* **0609** (2006) 066 [hep-th/0605017].

- [41] S. K. H. Auluck, “On the integral of the product of three bessel functions over an infinite domain,” *The Mathematica Journal*, 14 (2012).
- [42] S. i. Nam, “Parton-distribution functions for the pion and kaon in the gauge-invariant nonlocal chiral-quark model,” *Phys. Rev. D* **86** (2012) 074005 [arXiv:1205.4156 [hep-ph]].
- [43] R. E. Cutkosky, “Harmonic Functions and Matrix Elements for Hyperspherical Quantum Field Models,” *J. Math. Phys.* **25** (1984) 939.
- [44] O. Aharony, J. Marsano and M. Van Raamsdonk, “Two loop partition function for large N pure Yang-Mills theory on a small S^3 ,” *Phys. Rev. D* **74** (2006) 105012 [hep-th/0608156].
- [45] I. S. Gradshteyn and I. M. Ryzhik, “Table of Integrals, Series and Products,” Academic Press, 4th edition, 1980.
- [46] L. Y. Hung and Y. Shang, “On 1-loop diagrams in AdS space,” *Phys. Rev. D* **83** (2011) 024029 [arXiv:1007.2653 [hep-th]].